Journal of Computational Physics 490 (2023) 112290

Contents lists available at ScienceDirect

Journal of Computational Physics

journal homepage: www.elsevier.com/locate/jcp

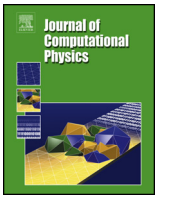

Two-level additive Schwarz methods for three-dimensional unsteady Stokes flows in patient-specific arteries with parameterized one-dimensional central-line coarse preconditioner ☆

Yingzhi Liu, Xiao-Chuan Cai *

Department of Mathematics, University of Macau, Macau

ARTICLE INFO

Article history:
Received 24 January 2022
Received in revised form 3 April 2023
Accepted 7 June 2023
Available online 22 June 2023

Keywords:
Unsteady Stokes problem
Blood flow in artery
Multilevel domain decomposition
Parameterized central-line coarse space
Finite element method

ABSTRACT

We consider the numerical solution of unsteady Stokes equations in patient-specific arterial-like domains in 3D. A Stokes-like solver is a necessary component in a more sophisticated nonlinear Navier-Stokes method, for which several multilevel domain decomposition methods have been introduced recently. Because of the complex geometry, the construction and the solve of the coarse problem usually take a large percentage of the total compute time. In this paper, we introduce a parameterized one-dimensional Stokes solver defined along the centerline of the artery and use its stabilized finite element discretization to construct a coarse preconditioner. With suitable 3D-to-1D restriction and 1D-to-3D extension operators on fully unstructured meshes, a two-level additive Schwarz preconditioner can be constructed. Some numerical experiments for flows in realistic arteries are presented to show the efficiency and robustness of the new coarse preconditioner whose computational cost is considerably lower than the existing three-dimensional coarse preconditioners.

1. Introduction

To understand and predict the behavior of blood flows in human body, numerical simulation is an important tool [1–8]. In the simulations, Navier-Stokes equations are often used to model the physics and the arterial geometry is reconstructed from medical images obtained with computer tomography (CT) or magnetic resonance imaging (MRI). In the Navier-Stokes solver, the most time consuming part of the computation is in the linear solver in which a Stokes-like system has to be constructed and solved at each time step. When solving such a problem on a parallel computer, a multilevel preconditioner is usually necessary to guarantee the scalability. As the number of subdomains increases the coarse solver in the preconditioner often takes a significantly percentage of the overall compute time. In this paper, we introduce and study a two-level additive Schwarz preconditioner for three-dimensional unsteady Stokes flows in patient-specific arteries, where

☆ This work was supported in part by FDCT 0141/2021/A3, 0079/2021/AFJ, and NSFC 12201658.
* Corresponding author.
E-mail addresses: yingzhiliu@um.edu.mo (Y. Liu), xccai@um.edu.mo (X.-C. Cai).

https://doi.org/10.1016/j.jcp.2023.112290
0021-9991/

the coarse preconditioner is constructed by a parameterized one-dimensional Stokes discretization on the centerline of the arterial domain. Comparing with existing three-dimensional coarse solvers, the cost of the one-dimensional solver is almost ignorable.

As the numerical computation is time-consuming for complex blood flows in three-dimensional arteries with lots of branches, reduced one-dimensional models [9–13] have been used for studying blood flows in arteries such as coronary arteries [14,15], arteries with stents or prostheses [16–18]. The one-dimensional model of the flow in an artery without bifurcation can be derived by integrating the continuous Navier-Stokes equations and applying certain model order reduction techniques across the axial section of the artery [2,11]. With reasonable bifurcation conditions, the one-dimensional model can be extended to bifurcating arteries [12–15]. In order to have high physical fidelity for the major arteries, A. Quarteroni et al. introduced a multiscale model of the entire circulatory system by coupling the three-dimensional model in the major arteries with zero, and one dimensional models in the minor arteries together [2,3,11,19]. We also mention another technique called hierarchical model reduction [20–23] consisting of different approximations of the dominant axial dynamics and the local transverse dynamics, more specifically, a piecewise-based [21] or isogeometry-based [23] approximation along the axial direction and a spectral approximation along the transverse direction with the Cartesian [21] or polar [22] coordinates, improving the accuracy of the one-dimensional model with a small increase in the number of degrees of freedom by capturing the transverse component with spectral methods. The basic mathematical assumption of the one-dimensional model is that the blood flow is more or less uniform across the axial section. The assumption is sometimes true in part of the artery, but not always true. In certain part of the artery when the flow is near chaotic, highly rotational, or when there is stenosis or aneurysm, only three-dimensional models can offer reasonably accuracy results. Although some one-dimensional models were numerically verified to be the reasonable representation of the three-dimensional model in many cases such as the diastole of the aorta [24] and the intracranial arterial networks [25], the large differences were also observed numerically in the systole of the aorta [24] and the cerebral circulation [26]. Limited by the characteristics of the one-dimensional model, it is usually used to study the global behavior of the spatially averaged pressure and flow waveforms such as the mechanisms underlying pulse wave propagation and the wave intensity analysis. For the localized hemodynamic quantities such as wall shear stress, and its gradient and the simulation of complex flows in, for examples, the patient-specific circle of Willis and the aneurysmal cerebral artery, the full three-dimensional model is essential [25,27].

For solving Stokes-like or saddle-point problems, several numerical methods were proposed such as Uzawa's methods [28,29], projection methods [30–33] and preconditioned Krylov subspace methods [34–38]. Uzawa's methods and projection methods split the velocity and pressure fields and solve the two subsystems individually, and solutions for the pressure and velocity are combined iteratively to form the solution of the original problem. Preconditioned Krylov subspace methods are to solve the full saddle-point system by Krylov subspace methods with a coupled or decoupled preconditioner. In [37,38], the fully coupled preconditioner is shown to be faster than the partially coupled and the fully decoupled preconditioners. We also mention there are some non-overlapping domain decomposition methods for saddle-point problems including BDDC methods [39,40] and dual-primal FETI methods [41,42].

In this paper, we focus on the unsteady Stokes problem defined on some realistic three-dimensional arterial domains and develop an effective and scalable two-level overlapping additive Schwarz preconditioner. Classical two-level methods with a coarse component offer good the scalability. However, due to the geometrical complexity of the artery, the coarse problem is often difficult to construct and time-consuming to solve, especially for arteries with many branches and for parallel computers with many processor cores. Although a geometry-preserving coarse mesh [43,44] is constructed and numerically verified to be effective to improve the scalability, the construction is too costly in terms of the user's time. Taking the advantage of cheap one-dimensional models, [45] presented a fully coupled two-level additive Schwarz preconditioner for the steady-state Stokes problems in two-dimensional artery-like domains. In [45] the coarse preconditioner was constructed by the finite element discretization of the one-dimensional Stokes model on the centerline of arterial-like domains and the restriction and interpolation operators were obtained based on a two-dimensional coarse mesh. In this work, we extend the central-line coarse preconditioner to the unsteady Stokes flows in three-dimensional realistic arteries with resistance outlet boundary conditions. Moreover, in order to remove the construction of the high-dimensional coarse mesh, the restriction and the interpolation operators between the three-dimensional finite element space and the one-dimensional central-line finite element space are constructed by the piecewise linear interpolation along the centerline and the radial basis interpolation along the cross sections. Numerical experiments show that the central-line coarse preconditioner has a very low computational cost and is highly effective in controlling the scalability of the overall algorithm. We also mention another application of the central-line coarse preconditioner for the general nonlinear Navier-Stokes equations found in [46].

The rest of the paper is organized as follows. In Section 2 we describe the model problem and the stabilized finite element discretization. In Section 3 we introduce the corresponding one-dimensional central-line model and its stabilized finite element discretization. In Section 4 we present the restriction and interpolation matrices, and the two-level additive Schwarz preconditioner with central-line coarse preconditioner. Finally we show some numerical experiments for some benchmark cases and also realistic arteries.

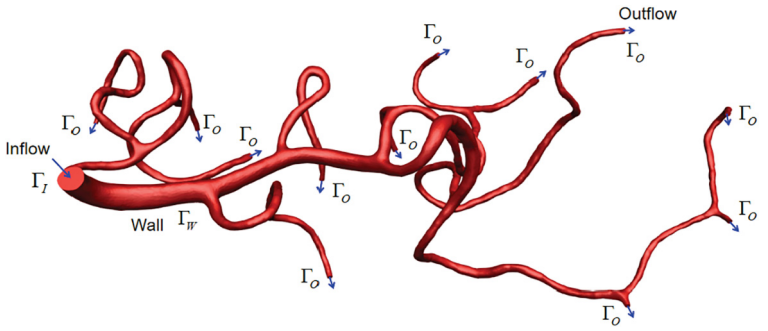

Fig. 1. A realistic cerebral artery with 1 inlet and 12 outlets.

2. Unsteady Stokes model and its stabilized finite element discretization

Consider the unsteady Stokes problem in an arterial domain $\Omega \in \mathbb{R}^3$ (see Fig. 1),

$$\begin{cases} \dfrac{\partial \boldsymbol{u}}{\partial t} - \nu \Delta \boldsymbol{u} + \nabla p = \boldsymbol{f} & \text{in} \quad \Omega \times (0,T), \\ \nabla \cdot \boldsymbol{u} = \boldsymbol{0} & \text{in} \quad \Omega \times (0,T), \\ \boldsymbol{u}(\boldsymbol{x},0) = \boldsymbol{u}_0(\boldsymbol{x}) & \text{in} \quad \Omega \times \{0\}, \end{cases} \tag{1}$$

where $\boldsymbol{u}$ is the velocity, p is the pressure. Denote the boundary of the domain by $\partial\Omega = \Gamma_I \cup \Gamma_O \cup \Gamma_W$, where Γ_I, Γ_W and Γ_O are the inlet boundary, the arterial wall and the outlet boundary, respectively. On the inlet boundary Γ_I, we impose the Dirichlet boundary condition on the velocity field

$$\boldsymbol{u} = \boldsymbol{u}_I \quad \text{on } \Gamma_I \times (0,T). \tag{2}$$

On the arterial wall, we impose the no slip boundary condition on the velocity field

$$\boldsymbol{u} = 0 \quad \text{on } \Gamma_W \times (0,T). \tag{3}$$

On the outlets $\{\Gamma_{Oi}\}_{i=1}^m$, we impose either the constant pressure boundary condition

$$p = p_i \quad \text{on } \Gamma_{Oi} \times (0,T), \tag{4}$$

or the resistance boundary condition

$$p = R_i Q_i \quad \text{on } \Gamma_{Oi} \times (0,T), \tag{5}$$

where p_i is the constant pressure, R_i is the constant resistance and $Q_i = \int_{\Gamma_{Oi}} \boldsymbol{u} \cdot \boldsymbol{n}$ is the fluid flux at the local outlet section Γ_{Oi}. Denote by $\boldsymbol{H}^1_W(\Omega) = \left\{\boldsymbol{v} \in \boldsymbol{H}^1(\Omega) : \boldsymbol{v}|_{\Gamma_I} = \boldsymbol{u}_I, \boldsymbol{v}|_{\Gamma_W} = 0\right\}$, $\boldsymbol{H}^1_{IW}(\Omega) = \left\{\boldsymbol{v} \in \boldsymbol{H}^1(\Omega) : \boldsymbol{v}|_{\Gamma_I \cup \Gamma_W} = 0\right\}$. Then the variational formulation of (1) with boundary conditions (2), (3) and (4) (or (5)) is to find $(\boldsymbol{u}(\cdot,t), p(\cdot,t)) \in \boldsymbol{H}^1_W(\Omega) \times L^2(\Omega)$ such that

$$\left(\frac{\partial \boldsymbol{u}}{\partial t}, \boldsymbol{v}\right) + a(\boldsymbol{u}, \boldsymbol{v}) + b(\boldsymbol{v}, p) + c(\boldsymbol{u}, \boldsymbol{v}, p) = f(\boldsymbol{v}),$$
$$b(\boldsymbol{u}, q) = 0, \quad \boldsymbol{u}(\boldsymbol{x}, 0) = \boldsymbol{u}_0(\boldsymbol{x}),$$

for all $\boldsymbol{v} \in \boldsymbol{H}^1_{IW}(\Omega), q \in L^2(\Omega)$ and $t \in (0,T)$, where $a(\cdot,\cdot), b(\cdot,\cdot), c(\cdot,\cdot,\cdot)$ and $f(\cdot)$ are defined as

$$a(\boldsymbol{u}, \boldsymbol{v}) = \int_\Omega \nu \nabla \boldsymbol{u} : \nabla \boldsymbol{v} \mathrm{d}\Omega, \quad b(\boldsymbol{v}, p) = -\int_\Omega p \nabla \cdot \boldsymbol{v} \mathrm{d}\Omega,$$
$$c(\boldsymbol{u}, \boldsymbol{v}, p) = -\int_{\Gamma_O} ((\nu \nabla \boldsymbol{u} \cdot \boldsymbol{n}) \cdot \boldsymbol{v} - p \boldsymbol{v} \cdot \boldsymbol{n}) \mathrm{d}\Gamma_O, \quad f(\boldsymbol{v}) = \int_\Omega \boldsymbol{f} \cdot \boldsymbol{v} \mathrm{d}\Omega.$$

Using the outlet boundary condition, $c(\boldsymbol{u}, \boldsymbol{v}, p)$ can be replaced by $c_\xi(\boldsymbol{u}, \boldsymbol{v})$ with

$$c_\xi(\boldsymbol{u}, \boldsymbol{v}) = -\int_{\Gamma_O} (\nu \nabla \boldsymbol{u} \cdot \boldsymbol{n}) \cdot \boldsymbol{v} \mathrm{d}\Gamma_O + \xi \sum_{i=1}^m R_i \int_{\Gamma_{Oi}} \boldsymbol{u} \cdot \boldsymbol{n} \mathrm{d}\Gamma_{Oi} \int_{\Gamma_{Oi}} \boldsymbol{v} \cdot \boldsymbol{n} \mathrm{d}\Gamma_{Oi} + (1-\xi) \sum_{i=1}^m \int_{\Gamma_{Oi}} p_i \boldsymbol{v} \cdot \boldsymbol{n} \mathrm{d}\Gamma_{Oi},$$

where $\xi = 0$ corresponds to the constant pressure boundary condition (4) and $\xi = 1$ corresponds to the resistance boundary condition (5).

Denote by $\mathcal{T}_h$ a conformal unstructured tetrahedral mesh of Ω and by S_h the continuous, piecewise linear polynomial function space on $\mathcal{T}_h$. Define the finite element spaces $\boldsymbol{V}_h = [S_h]^3 \cap \boldsymbol{H}^1_W(\Omega)$, $\boldsymbol{W}_h = [S_h]^3 \cap \boldsymbol{H}^1_{IW}(\Omega)$ for the velocity and $P_h = S_h \cap L^2(\Omega)$ for the pressure. For the finite element discretization, a stable finite element pair is required to satisfy the inf-sup condition or a stabilized finite element method is needed to circumvent this condition. Considering the computational complexity and the ease of implementation, we use a low- and equal-order stabilized finite element method [47,48] to spatially discretize the unsteady Stokes problem (1), that is, to find $(\boldsymbol{u}_h(\cdot,t), p_h(\cdot,t)) \in \boldsymbol{V}_h \times P_h$, such that

$$\left(\frac{\partial \boldsymbol{u}_h}{\partial t}, \boldsymbol{v}_h\right) + T_{\alpha\beta}\left(\frac{\partial \boldsymbol{u}_h}{\partial t}; \boldsymbol{v}_h, q_h\right) + S_{\alpha\beta}\left(\boldsymbol{u}_h, p_h; \boldsymbol{v}_h, q_h\right) = F_{\alpha\beta}\left(\boldsymbol{f}; \boldsymbol{v}_h, q_h\right),$$
$$(\boldsymbol{u}_h(\cdot,0), \boldsymbol{v}_h) = (\boldsymbol{u}_0, \boldsymbol{v}_h),$$

for all $\boldsymbol{v}_h \in \boldsymbol{W}_h, q_h \in P_h$ and $t \in (0,T)$, where

$$\begin{aligned}
S_\beta\left(\boldsymbol{u}_h, p_h; \boldsymbol{v}_h, q_h\right) &= a(\boldsymbol{u}_h, \boldsymbol{v}_h) + b(\boldsymbol{v}_h, p_h) + \beta b(\boldsymbol{u}_h, q_h) + c_\xi\left(\boldsymbol{u}_h, \boldsymbol{v}_h\right),\\
S_{\alpha\beta}\left(\boldsymbol{u}_h, p_h; \boldsymbol{v}_h, q_h\right) &= S_\beta\left(\boldsymbol{u}_h, p_h; \boldsymbol{v}_h, q_h\right) - \gamma \sum_{K\in\mathcal{T}_h} h_K^2(-\nu\Delta\boldsymbol{u}_h + \nabla p_h, -\alpha\Delta\boldsymbol{v}_h + \beta\nabla q_h)_K,\\
T_{\alpha\beta}\left(\frac{\partial \boldsymbol{u}_h}{\partial t}; \boldsymbol{v}_h, q_h\right) &= -\gamma \sum_{K\in\mathcal{T}_h} h_K^2\left(\frac{\partial \boldsymbol{u}_h}{\partial t}, -\alpha\Delta\boldsymbol{v}_h + \beta\nabla q_h\right)_K,\\
F_{\alpha\beta}\left(\boldsymbol{f}; \boldsymbol{v}_h, q_h\right) &= f(\boldsymbol{v}_h) - \gamma \sum_{K\in\mathcal{T}_h} h_K^2(\boldsymbol{f}, -\alpha\Delta\boldsymbol{v}_h + \beta\nabla q_h)_K,
\end{aligned}$$

with $\alpha \in \{-1, 0, 1\}$, $\beta \in \{-1, 1\}$ and $\gamma > 0$. Here h_K is the size of element K. Thanks to the linearity of $\boldsymbol{u}_h$ and $\boldsymbol{v}_h$ on each element K, the terms with $\Delta\boldsymbol{u}_h$ and $\Delta\boldsymbol{v}_h$ in $S_{\alpha\beta}, T_{\alpha,\beta}$ and $F_{\alpha\beta}$ vanish.

To discretize in time, we use the backward Euler method with uniform time step size Δt. Let $t^k = k\Delta t$ and $\boldsymbol{f}^k = \boldsymbol{f}(t^k)$. Given $\boldsymbol{u}_h^k$, the backward Euler step to obtain $\left(\boldsymbol{u}_h^{k+1}, p_h^{k+1}\right)$ can be described as

$$\frac{1}{\Delta t}\left(\boldsymbol{u}_h^{k+1} - \boldsymbol{u}_h^k, \boldsymbol{v}_h\right) + T_{\alpha\beta}\left(\frac{\boldsymbol{u}_h^{k+1} - \boldsymbol{u}_h^k}{\Delta t}; \boldsymbol{v}_h, q_h\right) + S_{\alpha\beta}\left(\boldsymbol{u}_h^{k+1}, p_h^{k+1}; \boldsymbol{v}_h, q_h\right) = F_{\alpha\beta}\left(\boldsymbol{f}^{k+1}; \boldsymbol{v}_h, q_h\right). \tag{6}$$

Set $\beta = -1$, (6) can be rewritten as

$$B_\xi\left(\boldsymbol{u}_h^{k+1}, p_h^{k+1}; \boldsymbol{v}_h, q_h\right) = F_\xi\left(\boldsymbol{u}_h^k; \boldsymbol{v}_h, q_h\right), \tag{7}$$

where

$$\begin{aligned}
B_\xi\left(\boldsymbol{u}_h^{k+1}, p_h^{k+1}; \boldsymbol{v}_h, q_h\right) =& \frac{1}{\Delta t}\left((\boldsymbol{u}_h^{k+1}, \boldsymbol{v}_h) + \gamma \sum_{K\in\mathcal{T}_h} h_K^2(\boldsymbol{u}_h^{k+1}, \nabla q_h)_K\right) + a\left(\boldsymbol{u}_h^{k+1}, \boldsymbol{v}_h\right) + b\left(\boldsymbol{v}_h, p_h^{k+1}\right)\\
&- b\left(\boldsymbol{u}_h^{k+1}, q_h\right) + \gamma \sum_{K\in\mathcal{T}_h} h_K^2\left(\nabla p_h^{k+1}, \nabla q_h\right)_K - \int_{\Gamma_O}\left(\nu\nabla\boldsymbol{u}_h^{k+1}\cdot\boldsymbol{n}\right)\cdot\boldsymbol{v}_h \mathrm{d}\Gamma_O\\
&+ \xi\sum_{i=1}^m R_i \int_{\Gamma_{Oi}} \boldsymbol{u}_h^{k+1}\cdot\boldsymbol{n}\mathrm{d}\Gamma_{Oi}\int_{\Gamma_{Oi}} \boldsymbol{v}_h\cdot\boldsymbol{n}\mathrm{d}\Gamma_{Oi},
\end{aligned} \tag{8}$$

$$\begin{aligned}
F_\xi(\boldsymbol{u}_h^k; \boldsymbol{v}_h, q_h) =& \frac{1}{\Delta t}\left(\left(\boldsymbol{u}_h^k, \boldsymbol{v}_h\right) + \gamma \sum_{K\in\mathcal{T}_h} h_K^2\left(\boldsymbol{u}_h^k, \nabla q_h\right)_K\right) + (\boldsymbol{f}^{k+1}, \boldsymbol{v}_h) + \gamma \sum_{K\in\mathcal{T}_h} h_K^2(\boldsymbol{f}^{k+1}, \nabla q_h)_K\\
&+ (\xi - 1)\sum_{i=1}^m \int_{\Gamma_{Oi}} p_i \boldsymbol{v}_h\cdot\boldsymbol{n}\mathrm{d}\Gamma_{Oi}.
\end{aligned} \tag{9}$$

Remark 2.1. We remark that because of the last integral term of B_ξ in (8), the stiffness matrix has some dense blocks corresponding to the resistance boundary condition ($\xi = 1$) at the outlets.

Below we show that the bilinear form just defined is coercive in the finite element spaces.

Theorem 2.1. *For any $\boldsymbol{u}_h \in \boldsymbol{W}_h$ and $p_h \in P_h$, we have*

$$B_\xi(\boldsymbol{u}_h, p_h; \boldsymbol{u}_h, p_h) \geq \left(\frac{h_{\min}^2}{C_I^2}\left(\frac{1}{2\Delta t} - C_r\nu\right) + (1-C_r)\nu\right)\|\nabla \boldsymbol{u}_h\|_0^2 + \gamma\left(1 - \frac{\gamma h_{\max}^2}{2\Delta t}\right)\|p_h\|_{0,h}^2, \tag{10}$$

where $h_{\min} = \min_{K\in\mathcal{T}_h}(h_K)$, $h_{\max} = \max_{K\in\mathcal{T}_h}(h_K)$ and $\|p_h\|_{0,h} = \left(\sum_K h_K^2 \|\nabla p_h\|_{0,K}^2\right)^{1/2}$ is a mesh-dependent norm of P_h.

Proof. From (8), we obtain

$$\begin{aligned} B_\xi(\boldsymbol{u}_h, p_h; \boldsymbol{u}_h, p_h) =& \frac{1}{\Delta t}\left(\|\boldsymbol{u}_h\|_0^2 + \sum_{K\in\mathcal{T}_h}\left(\boldsymbol{u}_h, \gamma h_K^2 \nabla p_h\right)_K\right) + \nu\|\nabla \boldsymbol{u}_h\|_0^2 + \gamma\|p_h\|_{0,h}^2 \\ & - \int_{\Gamma_O}(\nu\nabla \boldsymbol{u}_h\cdot\boldsymbol{n})\cdot\boldsymbol{u}_h \mathrm{d}\Gamma_O + \xi\sum_{i=1}^m R_i\left(\int_{\Gamma_{Oi}}\boldsymbol{u}_h\cdot\boldsymbol{n}\mathrm{d}\Gamma_{Oi}\right)^2. \end{aligned}$$

Using the Cauchy-Schwarz inequality, we have

$$\begin{aligned} \sum_{K\in\mathcal{T}_h}(\boldsymbol{u}_h, \gamma h_K^2\nabla p_h)_K &\leq \sum_{K\in\mathcal{T}_h}\left(\frac{1}{2}\|\boldsymbol{u}_h\|_{0,K}^2 + \frac{\gamma^2 h_K^2}{2} h_K^2\|\nabla p_h\|_{0,K}^2\right) \\ &\leq \frac{1}{2}\|\boldsymbol{u}_h\|_0^2 + \frac{\gamma^2 h_{\max}^2}{2}\|p_h\|_{0,h}^2. \end{aligned} \tag{11}$$

Using the trace theorem [49,50], we get

$$\int_{\Gamma_O}(\nu\nabla \boldsymbol{u}_h\cdot\boldsymbol{n})\cdot\boldsymbol{u}_h\mathrm{d}\Gamma_O \leq \nu\|\nabla \boldsymbol{u}_h\cdot\boldsymbol{n}\|_{-1/2,\Gamma_O}\|\boldsymbol{u}_h\|_{1/2,\Gamma_O} \leq C_r\nu\|\boldsymbol{u}_h\|_1^2, \tag{12}$$

where C_r is a constant depending on Ω. Combining (11) and (12) we have

$$B_\xi(\boldsymbol{u}_h, p_h; \boldsymbol{u}_h, p_h) \geq \left(\frac{1}{2\Delta t} - C_r\nu\right)\|\boldsymbol{u}_h\|_0^2 + (\nu - C_r\nu)\|\nabla \boldsymbol{u}_h\|_0^2 + \gamma\left(1 - \frac{\gamma h_{\max}^2}{2\Delta t}\right)\|p_h\|_{0,h}^2.$$

By using the inverse inequality $\|\nabla \boldsymbol{u}_h\|_{0,K} \leq C_I h_K^{-1}\|\boldsymbol{u}_h\|_{0,K}$, we obtain (10). □

Remark 2.2. To satisfy the spatial stability condition for the fully discretized problem, a sufficient condition based on Theorem 2.1 is to require

$$\frac{h_{\min}^2}{C_I^2}\left(\frac{1}{2\Delta t} - C_r\nu\right) + (1-C_r)\nu \geq C_1,\ 1 - \frac{\gamma h_{\max}^2}{2\Delta t} \geq C_2,$$

where $C_1, C_2 > 0$ should be independent of the spatial and temporal sizes, as well as γ. For sufficiently small Δt, the first condition holds easily. For the second condition, it holds if

$$h_{\max}^2 < \frac{2\Delta t}{\gamma}. \tag{13}$$

From the numerical results in [47,48], the stabilization parameter $\gamma = 0.04$ or $\gamma = 0.05$ was confirmed to be a good choice.

3. A parameterized one-dimensional Stokes model in 3D and its stabilized finite element discretization

In this section, we first recall the one-dimensional Stokes model and then introduce its stabilized finite element discretization in order to construct the central-line coarse preconditioner.

3.1. Parameterized one-dimensional Stokes model

To derive the parameterized one-dimensional Stokes model, we first restrict our attention to a non-branching artery Ω and assume that the artery is axial symmetric with respect to the centerline denoted by Ω^{cl}. Denote L as the arc length of Ω^{cl}, $\boldsymbol{x}_0$ as the start point corresponding to the inlet and $\boldsymbol{x}_1$ as the end point corresponding to the outlet. For any point $\boldsymbol{x} \in \Omega^{cl}$, let s be the arc length of the centerline from $\boldsymbol{x}_0$ to $\boldsymbol{x}$. For any $s \in [0, L]$, let $C_s(s)$ be the cross section of Ω, $A_s(s)$ the corresponding area and $r_0(s)$ the radius of $C_s(s)$. Further, we assume that the pressure is a constant on each cross section, the velocity components orthogonal to the centerline are negligible compared to the component u_s along the centerline, i.e., $\boldsymbol{u} \approx u_s \boldsymbol{\tau}$, where $\boldsymbol{\tau} = (\tau^1, \tau^2, \tau^3)$ is the unit tangent vector along the centerline and the component u_s can be expressed as

$$u_s(t, r, s) = u^{cl}(t, s)\zeta\left(\frac{r}{r_0(s)}\right). \tag{14}$$

Here $u^{cl}(t, s) = u_s(t, 0, s)$ is the value of u_s on the centerline and $\zeta(y) = (1 - y^2)$ $(y \in [0, 1])$ is a parabolic profile function, and $r \le r_0(s)$ is the radial coordinate with respect to $C_s(s)$. Let $\bar{u}_s = A_s^{-1} \int_{C_s} u_s \mathrm{d}C_s$ and $Q = \int_{C_s} u_s \mathrm{d}C_s = A_s \bar{u}_s$ be the mean velocity and the flux on C_s, respectively. Then from (14) we have $\bar{u}_s = u^{cl}/2$ and $Q = A_s u^{cl}/2$. Similarly, we define $p^{cl}(t, s)$ as the value of the pressure on the centerline.

Based on the above assumptions, following [2,45], we derive the parameterized 1D unsteady Stokes model from (1) in a single blood vessel which refers to an artery with one inlet, one outlet, and no bifurcation

$$\begin{cases} \dfrac{A_s}{2}\dfrac{\partial u^{cl}}{\partial t} + \dfrac{K_r}{2}u^{cl} + A_s\dfrac{\partial p^{cl}}{\partial s} = f^{cl}, \\ \dfrac{\partial (A_s u^{cl})}{\partial s} = 0, \ u^{cl}(s, 0) = u_0^{cl}(s), \end{cases} \tag{15}$$

where $K_r = 8\pi\nu$, $f^{cl} = \int_{C_s} \boldsymbol{f} \cdot \boldsymbol{\tau} \mathrm{d}C_s$ and $u_0^{cl} = \int_{C_s} \boldsymbol{u}_0 \cdot \boldsymbol{\tau} \mathrm{d}C_s$. By integrating (2), (4) and (5) on the corresponding boundary, we obtain the inlet velocity boundary condition

$$u^{cl}(0, t) = -\frac{2}{|\Gamma_I|}\int_{\Gamma_I} \boldsymbol{u}_I \cdot \boldsymbol{n} \mathrm{d}\Gamma_I := u_I^{cl}, \tag{16}$$

and the outlet constant pressure boundary condition

$$p^{cl}(s_{Oi}, t) = \frac{1}{|\Gamma_{Oi}|}\int_{\Gamma_{Oi}} p_i \mathrm{d}\Gamma_{Oi} = p_i, \tag{17}$$

or the outlet resistance boundary condition

$$p^{cl}(s_{Oi}, t) = R_i Q_i \approx R_i A_s(s_{Oi})\bar{u}_s = \frac{R_i A_s(s_{Oi})}{2} u^{cl}(s_{Oi}, t). \tag{18}$$

For general arteries with bifurcations, we can divide it into some single vessels. For simplicity, we assume that on each bifurcation there is one inflow vessel and two outflow vessels connected with it (see the top-right sub-figure in Fig. 2). On each bifurcation, using the conservation of flux and the continuity of the pressure [13,45], we obtain the following bifurcation compatibility conditions

$$Q_1 = Q_2 + Q_3, \quad p_1^{cl} = p_2^{cl} = p_3^{cl}, \tag{19}$$

or

$$A_{s_1} u_1^{cl} = A_{s_2} u_2^{cl} + A_{s_3} u_3^{cl}, \quad p_1^{cl} = p_2^{cl} = p_3^{cl}, \tag{20}$$

by using the fact $Q_i = \dfrac{A_{s_i}}{2} u_i^{cl}, i = 1, 2, 3$. For more general bifurcations involving more than two outflow vessels, similar bifurcation compatibility conditions can be derived.

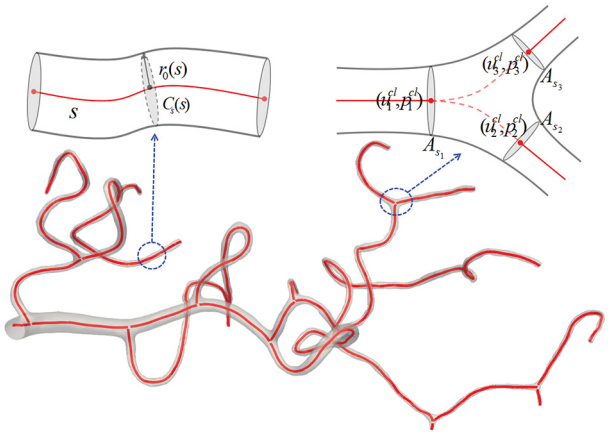

Fig. 2. Central line of an artery with cross sections at regular and bifurcating points.

3.2. Stabilized finite element discretization of parameterized one-dimensional Stokes model

Let $D \subset \mathbb{R}^3$ be a curve without branches, $L(D)$ its arc length and assume it has two endpoints $\boldsymbol{x}_0(D), \boldsymbol{x}_1(D)$. For any $\boldsymbol{x} \in D$, define a bijective map $X_D : [0, L(D)] \mapsto D$ as

$$X_D(s) = \boldsymbol{x},$$

where s is the arc length along D from $\boldsymbol{x}_0(D)$ to $\boldsymbol{x}$.

For the centerline Ω^{cl}, we denote n_J and n_{cl} as the number of its bifurcations and its branches, respectively, define Ω_i^{cl} as its ith branch and C_s^i as the cross section of Ω at s on Ω_i^{cl}. Let $J_k = \{J_k^0, J_k^1, J_k^2\}$ be an index set where J_k^0, J_k^1 and J_k^2 are the indexes of the inflow branch and two outflow branches connected with the kth bifurcation, respectively. For simplicity, we denote $\boldsymbol{x}_i^0 = \boldsymbol{x}_0(\Omega_i^{cl})$ and $\boldsymbol{x}_i^1 = \boldsymbol{x}_1(\Omega_i^{cl})$ as the inlet and outlet of Ω_i^{cl}, and $s_i^0 = 0$ and $s_i^1 = L(\Omega_i^{cl})$ as the arc lengths of Ω_i^{cl} corresponding to $\boldsymbol{x}_i^0$ and $\boldsymbol{x}_i^1$. Specifically, denote Ω_I^{cl} and Ω_{Oj}^{cl} as the inlet and outlet branches of the centerline Ω^{cl}, $s_I = 0$ and $s_{Oj} = L(\Omega_{Oj}^{cl})$, $j = 1, \ldots, m$ as the arc lengths corresponding to the inlet and outlet of Ω^{cl}. With these definitions, for any $\boldsymbol{x} \in \Omega_i^{cl}$, there exists $s \in (0, L(\Omega_i^{cl}))$, such that $\boldsymbol{x} \in X_{\Omega_i^{cl}}(s)$. Moreover, we have $\Omega^{cl} = \bigcup_{i=1}^{n_{cl}} \Omega_i^{cl}$, and for any $\boldsymbol{x} \in \Omega$, there exists $i \in \{1, \ldots, n_{cl}\}$ and $s \in (0, L(\Omega_i^{cl}))$, such that $\boldsymbol{x} \in C_s^i(s)$. On each branch Ω_i^{cl}, denote u_i^{cl}, p_i^{cl} and A_s^i as the velocity, the pressure and the cross-sectional area. Then the velocity u^{cl}, the pressure p^{cl} and the cross-sectional area A_s in Ω^{cl} can be piecewise defined by

$$u^{cl}|_{\Omega_i^{cl}} = u_i^{cl}, \quad p^{cl}|_{\Omega_i^{cl}} = p_i^{cl}, \quad A_s|_{\Omega_i^{cl}} = A_s^i. \ (i = 1, \ldots, n_{cl})$$

For the velocity field on the centerline Ω^{cl}, we define

$$\mathbf{M}(\Omega^{cl}) = \Big\{ v^{cl}|_{\Omega_i^{cl}} \in H^1(\Omega_i^{cl}) : v^{cl}(s_I)|_{\Omega_I^{cl}} = u_I^{cl},\ A_s(s_{J_k^0}^1) v^{cl}(s_{J_k^0}^1)|_{\Omega_{J_k^0}^{cl}} = A_s(s_{J_k^1}^0) v^{cl}(s_{J_k^1}^0)|_{\Omega_{J_k^1}^{cl}}$$
$$+ A_s(s_{J_k^2}^0) v^{cl}(s_{J_k^2}^0)|_{\Omega_{J_k^2}^{cl}},\ i = 1, \ldots, n_{cl},\ k = 1, \ldots, n_J \Big\},$$

$$\mathbf{M}_0(\Omega^{cl}) = \Big\{ v^{cl}|_{\Omega_i^{cl}} \in H^1(\Omega_i^{cl}) : v^{cl}(s_I)|_{\Omega_I^{cl}} = 0,\ v^{cl}(s_{J_k^0}^1)|_{\Omega_{J_k^0}^{cl}} = 0,\ i = 1, \ldots, n_{cl},\ k = 1, \ldots, n_J \Big\},$$

where the velocity in $\mathbf{M}(\Omega^{cl})$ satisfies the Dirichlet boundary condition (16) at the inlet and the flux conservation condition of (20) at all bifurcations. The space $\mathbf{M}_0(\Omega^{cl})$ with the homogeneous boundary conditions at the inlets of the centerline and all bifurcations is used as the test function space. For the pressure field on the centerline Ω^{cl}, we define

$$\mathbf{Q}(\Omega^{cl}) = \Big\{ q^{cl}|_{\Omega_i^{cl}} \in L^2(\Omega_i^{cl}) : q^{cl}(s_{J_k^1}^0)|_{\Omega_{J_k^1}^{cl}} = p^{cl}(s_{J_k^0}^1)|_{\Omega_{J_k^0}^{cl}},\ q^{cl}(s_{J_k^2}^0)|_{\Omega_{J_k^2}^{cl}} = p^{cl}(s_{J_k^0}^1)|_{\Omega_{J_k^0}^{cl}},$$
$$q^{cl}(s_{Oj})|_{\Omega_{Oj}^{cl}} = p_j,\ i = 1, \ldots, n_{cl},\ j = 1, \ldots, m,\ k = 1, \ldots, n_J \Big\},\ (\xi = 0),$$

$$\mathbf{Q}_0(\Omega^{cl}) = \Big\{ q^{cl}|_{\Omega_i^{cl}} \in L^2(\Omega_i^{cl}) : q^{cl}(s^0_{J_k^1})|_{\Omega^{cl}_{J_k^1}} = 0,\ q^{cl}(s^0_{J_k^2})|_{\Omega^{cl}_{J_k^2}} = 0,\ q^{cl}(s_{Oj})|_{\Omega^{cl}_{Oj}} = 0,$$
$$i = 1, \ldots, n_{cl},\ j = 1, \ldots, m,\ k = 1, \ldots, n_J \Big\},\ (\xi = 0),$$

for $\xi = 0$, where the pressure in $\mathbf{Q}(\Omega^{cl})$ satisfies the constant pressure boundary condition (17) at the outlets and the pressure continuity condition of (20) at all bifurcations. The space $\mathbf{Q}_0(\Omega^{cl})$ with the homogeneous boundary conditions at the outlets of the centerline and all bifurcations is used as the test function space. Similarly for $\xi = 1$, we define

$$\mathbf{Q}(\Omega^{cl}) = \Big\{ q^{cl}|_{\Omega_i^{cl}} \in L^2(\Omega_i^{cl}) : q^{cl}(s^0_{J_k^1})|_{\Omega^{cl}_{J_k^1}} = p^{cl}(s^1_{J_k^0})|_{\Omega^{cl}_{J_k^0}},\ q^{cl}(s^0_{J_k^2})|_{\Omega^{cl}_{J_k^2}} = p^{cl}(s^1_{J_k^0})|_{\Omega^{cl}_{J_k^0}},$$
$$i = 1, \ldots, n_{cl},\ k = 1, \ldots, n_J \Big\},\ (\xi = 1),$$
$$\mathbf{Q}_0(\Omega^{cl}) = \Big\{ q^{cl}|_{\Omega_i^{cl}} \in L^2(\Omega_i^{cl}) : q^{cl}(s^0_{J_k^1})|_{\Omega^{cl}_{J_k^1}} = 0,\ q^{cl}(s^0_{J_k^2})|_{\Omega^{cl}_{J_k^2}} = 0,\ i = 1, \ldots, n_{cl},$$
$$k = 1, \ldots, n_J \Big\},\ (\xi = 1),$$

where the pressure in $\mathbf{Q}(\Omega^{cl})$ satisfies the pressure continuity condition of (20) at all bifurcations. The space $\mathbf{Q}_0(\Omega^{cl})$ with the homogeneous boundary conditions at the outlets of all bifurcations is used as the test function space. As the velocity in $\mathbf{M}(\Omega^{cl})$ and the pressure in $\mathbf{Q}(\Omega^{cl})$ are not required to satisfy the resistance boundary condition (18), the condition needs to be added and imposed additionally in the weak formulation.

The variational formulation of the parameterized one-dimensional Stokes problem on the centerline is to find $(u^{cl}(\cdot,t),\ p^{cl}(\cdot,t)) \in \mathbf{M}(\Omega^{cl}) \times \mathbf{Q}(\Omega^{cl})$ such that

$$\left(\frac{A_s}{2}\frac{\partial u^{cl}}{\partial t}, v^{cl}\right) + a^{cl}(u^{cl}, v^{cl}) + b^{cl}(v^{cl}, p^{cl}) = f^{cl}(v^{cl}),$$
$$b^{cl}(u^{cl}, q^{cl}) - c^{cl}(u^{cl}, q^{cl}) = 0, \quad u^{cl}(s,0) = u_0^{cl}(s),$$

for all $v^{cl} \in \mathbf{M}_0(\Omega^{cl}), q^{cl} \in \mathbf{Q}_0(\Omega^{cl})$ and $t \in (0,T)$, where $a_{cl}(\cdot,\cdot), b_{cl}(\cdot,\cdot), c_{cl}(\cdot,\cdot)$ and $f_{cl}(\cdot)$ are defined by

$$a^{cl}(u^{cl}, v^{cl}) = \int_{\Omega^{cl}} \frac{K_r}{2} u^{cl} v^{cl} \mathrm{d}s, \quad b^{cl}(u^{cl}, q^{cl}) = \int_{\Omega^{cl}} A_s u^{cl} \frac{\partial q^{cl}}{\partial s} \mathrm{d}s,$$
$$c^{cl}(u^{cl}, q^{cl}) = \sum_{i=1}^{n_{cl}} A_s u^{cl} q^{cl}\Big|_{s_i^0}^{s_i^1}, \quad f^{cl}(v^{cl}) = \int_{\Omega^{cl}} f^{cl} v^{cl} \mathrm{d}s.$$

Using the inlet and outlet boundary conditions (16)–(18), $c^{cl}(u^{cl}, q^{cl})$ can be rewritten as

$$c_\xi^{cl}(u^{cl}, q^{cl}) = -A_s(s_I) u_I^{cl} q^{cl}(s_I)|_{\Omega_I^{cl}} + \sum_{k=1}^{n_J} A_s(s^1_{J_k^0}) u^{cl}(s^1_{J_k^0}) q^{cl}(s^1_{J_k^0})|_{\Omega^{cl}_{J_k^0}} + \xi \sum_{j=1}^{m} \frac{2}{R_i} p^{cl}(s_{Oj}) q^{cl}(s_{Oj})|_{\Omega^{cl}_{Oj}},$$

where $\xi = 0$ corresponds to the constant pressure boundary condition and $\xi = 1$ corresponds to the resistance boundary condition.

We introduce a polyline mesh $\mathcal{T}_H^{cl}$ with the mesh size $O(H)$ for Ω^{cl} and the corresponding continuous, piecewise linear polynomial function space S_H^{cl}. We require that all end points of branches are mesh points to ensure the overall mesh is conformal. For each branch Ω_i^{cl}, the mesh $\mathcal{T}_H^{cl,i}$ and the space $S_H^{cl,i}$ can be derived from the restriction of the mesh $\mathcal{T}_H^{cl}$ and the space S_H^{cl} on Ω_i^{cl}, i.e., $\mathcal{T}_H^{cl,i} = \mathcal{T}_H^{cl}(\Omega_i^{cl})$, $S_H^{cl,i} = S_H^{cl}(\Omega_i^{cl})$. Define the finite element spaces $V_H^{cl} = S_H^{cl} \cap \mathbf{M}(\Omega^{cl})$, $W_H^{cl} = S_H^{cl} \cap \mathbf{M}_0(\Omega^{cl})$ for the velocity and $P_H^{cl} = S_H^{cl} \cap \mathbf{Q}(\Omega^{cl})$, $Q_H^{cl} = S_H^{cl} \cap \mathbf{Q}_0(\Omega^{cl})$ for the pressure. A stabilized finite element method to spatially discretize the unsteady 1D Stokes problem can be described as: find $(u_H^{cl}(\cdot,t),\ p_H^{cl}(\cdot,t)) \in V_H^{cl} \times P_H^{cl}$, such that

$$\left(\frac{A_s}{2}\frac{\partial u_H^{cl}}{\partial t}, v_H^{cl}\right) + T_{\alpha\beta}^{cl}\left(\frac{\partial u_H^{cl}}{\partial t}; v_H^{cl}, q_H^{cl}\right) + S_{\alpha\beta}^{cl}\left(u_H^{cl}, p_H^{cl}; v_H^{cl}, q_H^{cl}\right) = F_{\alpha\beta}^{cl}\left(v_H^{cl}, q_H^{cl}\right), \tag{21}$$
$$\left(u_H^{cl}(\cdot,0), v_H^{cl}\right) = \left(u_0^{cl}, v_H^{cl}\right), \tag{22}$$

for all $v_H^{cl} \in W_H^{cl}, q_H^{cl} \in Q_H^{cl}$ and $t \in (0, T)$, where

$$S_\beta^{cl}\left(u_H^{cl}, p_H^{cl}; v_H^{cl}, q_H^{cl}\right) = a^{cl}\left(u_H^{cl}, v_H^{cl}\right) + b\left(v_H^{cl}, p_H^{cl}\right) + \beta b\left(u_H^{cl}, q_H^{cl}\right) - \beta c_\xi^{cl}\left(u_H^{cl}, q_H^{cl}\right),$$

$$S_{\alpha\beta}^{cl}\left(u_H^{cl}, p_H^{cl}; v_H^{cl}, q_H^{cl}\right) = S_\beta^{cl}\left(u_H^{cl}, p_H^{cl}; v_H^{cl}, q_H^{cl}\right) - \gamma^{cl}\sum_{e\in\mathcal{T}_H^{cl}} H_e^2\left(\frac{K_r}{2}u_H^{cl} + A_s\frac{\partial p_H^{cl}}{\partial s}, \alpha v_H^{cl} + \beta\frac{\partial q_H^{cl}}{\partial s}\right)_e,$$

$$T_{\alpha\beta}^{cl}\left(\frac{\partial u_H^{cl}}{\partial t}; v_H^{cl}, q_H^{cl}\right) = -\gamma^{cl}\sum_{e\in\mathcal{T}_H^{cl}} H_e^2\left(\frac{A_s}{2}\frac{\partial u_H^{cl}}{\partial t}, \alpha v_H^{cl} + \beta\frac{\partial q_H^{cl}}{\partial s}\right)_e,$$

$$F_{\alpha\beta}^{cl}\left(v_H^{cl}, q_H^{cl}\right) = f^{cl}\left(v_H^{cl}\right) - \gamma^{cl}\sum_{e\in\mathcal{T}_H^{cl}} H_e^2\left(f^{cl}, \alpha v_H^{cl} + \beta\frac{\partial q_H^{cl}}{\partial s}\right)_e$$

with $\alpha \in \{-1, 0, 1\}, \beta \in \{-1, 1\}$ and the stabilization parameter $\gamma^{cl} > 0$. Set $\alpha = 0, \beta = -1$ and use backward Euler method on time to obtain the fully discretized 1D Stokes scheme at t^{k+1} for given $u_H^{cl,k}$:

$$B_\xi^{cl}\left(u_H^{cl,k+1}, p_H^{cl,k+1}; v_H^{cl}, q_H^{cl}\right) = F_\xi^{cl}\left(u_H^{cl,k}; v_H^{cl}, q_H^{cl}\right), \tag{23}$$

where

$$\begin{aligned} B_\xi^{cl}\left(u_H^{cl,k+1}, p_H^{cl,k+1}; v_H^{cl}, q_H^{cl}\right) &= \frac{1}{\Delta t}\left(\frac{A_s}{2}u_H^{cl,k+1}, v_H^{cl}\right) + a^{cl}\left(u_H^{cl,k+1}, v_H^{cl}\right) + b\left(v_H^{cl}, p_H^{cl,k+1}\right) \\ &- b\left(u_H^{cl,k+1}, q_H^{cl}\right) + \sum_{k=1}^{n_J} A_s(s_{J_k^0}^1)u^{cl}(s_{J_k^0}^1)q^{cl}(s_{J_k^0}^1)|_{\Omega_{J_k^0}^{cl}} + \xi\sum_{j=1}^{m}\frac{2}{R_i}p^{cl}(s_{Oj})q^{cl}(s_{Oj})|_{\Omega_{Oj}^{cl}} \\ &+ \gamma^{cl}\sum_{e\in\mathcal{T}_H^{cl}} H_e^2\left(\frac{A_s}{2\Delta t}u_H^{cl,k+1} + \frac{K_r}{2}u_H^{cl,k+1} + A_s\frac{\partial p_H^{cl,k+1}}{\partial s}, \frac{\partial q_H^{cl}}{\partial s}\right)_e, \end{aligned} \tag{24}$$

$$\begin{aligned} F_\xi^{cl}(u_H^{cl,k}; v_H^{cl}, q_H^{cl}) &= \frac{1}{\Delta t}\left(\frac{A_s}{2}u_H^{cl,k}, v_H^{cl}\right) + \left(f^{cl,k+1}, v_H^{cl}\right) + A_s(s_I)u_I^{cl}(s_I)q_H^{cl}(s_I)|_{\Omega_I^{cl}} \\ &+ \gamma^{cl}\sum_{e\in\mathcal{T}_H^{cl}} H_e^2\left(\frac{A_s}{2\Delta t}u_H^{cl,k} + f^{cl,k+1}, \frac{\partial q_H^{cl}}{\partial s}\right)_e. \end{aligned} \tag{25}$$

Remark 3.1. In (24), the last term is a stabilization term derived from the stabilized part of $S_{\alpha,\beta}^{cl}$ and $T_{\alpha,\beta}^{cl}$ and other terms come from S_β^{cl}. For $\xi = 1$, the resistance boundary condition (18) is needed to replace the corresponding equations of (23) which match the degrees of freedom of the velocity or the pressure at the outlets.

Below we show that under certain conditions on the temporal and spatial mesh sizes, the problem defined in (23) is solvable.

Theorem 3.1. *For any $u_H^{cl} \in W_H^{cl}$ and $p_H^{cl} \in Q_H^{cl}$, we have*

$$B_\xi^{cl}\left(u_H^{cl}, p_H^{cl}; u_H^{cl}, p_H^{cl}\right) \geq \left(\frac{3}{8\Delta t} - \frac{\Delta t K_r^2}{8A_{\min}^2}\right)\left\|u_H^{cl}\right\|_{0,A_s}^2 + \frac{K_r}{4}\left\|u_H^{cl}\right\|_0^2 + \gamma^{cl}\left(1 - \frac{\gamma^{cl}H_{\max}^2}{2\Delta t}\right)\left\|p_H^{cl}\right\|_{0,A_s,H}^2, \tag{26}$$

where $H_{\max} = \max_{e\in\mathcal{T}_H^{cl}} H_e$, $A_{\min} = \min_{s\in\Omega^{cl}} A_s$, $\left\|u_H^{cl}\right\|_{0,A_s} = \left\|A_s^{1/2}u_H^{cl}\right\|_{0,\Omega^{cl}}$ is a geometry-dependent norm of W_H^{cl} and $\left\|p_H^{cl}\right\|_{0,A_s,H} = \left(\sum_e H_e^2\left\|A_s^{1/2}\frac{\partial p_H^{cl}}{\partial s}\right\|_{0,e}^2\right)^{1/2}$ is a mesh-dependent norm of P_H^{cl}.

Proof. From (24), we obtain

$$B_\xi^{cl}\left(u_H^{cl}, p_H^{cl}; u_H^{cl}, p_H^{cl}\right) = \frac{1}{\Delta t}\left(\frac{1}{2}\left\|u_H^{cl}\right\|_{0,A_s}^2 + \sum_{e\in\mathcal{T}_H^{cl}}\left(\left(\frac{A_s}{2} + \frac{\Delta t K_r}{2}\right)u_H^{cl}, \gamma^{cl}H_e^2\frac{\partial p_H^{cl}}{\partial s}\right)_e\right)$$

$$+\frac{K_r}{2}\left\|u_H^{cl}\right\|_0^2+\gamma^{cl}\left\|p_H^{cl}\right\|_{0,A_s,H}^2+\xi\sum_{j=1}^{m}\frac{2}{R_i}\left(p^{cl}(s_{Oj})|_{\Omega_{Oj}^{cl}}\right)^2. \tag{27}$$

Using the Cauchy-Schwarz inequality, we have

$$\begin{aligned}
&\sum_{e\in\mathcal{T}_H^{cl}}\left(\left(\frac{A_s}{2}+\frac{\Delta tK_r}{2}\right)u_H^{cl},\gamma^{cl}H_e^2\frac{\partial p_H^{cl}}{\partial s}\right)_e\\
&\le\sum_{e\in\mathcal{T}_H^{cl}}\left(\frac{1}{2}\left(\left(\frac{\sqrt{A_s}}{2}+\frac{\Delta tK_r}{2\sqrt{A_s}}\right)^2u_H^{cl},u_H^{cl}\right)_e+\frac{\left(\gamma^{cl}\right)^2H_e^2}{2}H_e^2\left(A_s\frac{\partial p_H^{cl}}{\partial s},\frac{\partial p_H^{cl}}{\partial s}\right)_e\right)\\
&\le\frac{1}{8}\left\|u_H^{cl}\right\|_{0,A_s}^2+\frac{\Delta tK_r}{4}\left\|u_H^{cl}\right\|_0^2+\left(\frac{(\Delta tK_r)^2}{8A_s}u_H^{cl},u_H^{cl}\right)+\frac{\left(\gamma^{cl}\right)^2H_{\max}^2}{2}\left\|p_H^{cl}\right\|_{0,A_s,H}^2.
\end{aligned}\tag{28}$$

Combining (27) with (28), we obtain (26). □

Remark 3.2. Theorem 3.1 implies similar sufficient stability conditions for h, Δt and γ^{cl}

$$\frac{3}{8\Delta t}-\frac{\Delta tK_r^2}{8A_{\min}^2}\ge 0,\ 1-\frac{\gamma^{cl}H_{\max}^2}{2\Delta t}>C_3,$$

where $C_3>0$ is independent of h, Δt and γ^{cl}. Analogously the first inequality is easy to satisfy for a sufficiently small Δt and the second inequality requires $H_{\max}^2<2\Delta t/\gamma^{cl}$.

To show roughly how the 1D model behaves, in Fig. 3, we present some computed velocity and pressure curves of (23) with a periodic velocity boundary condition at the inlet of the centerline of a two-branch artery given in the mid figure of Fig. 7. The top figures in Fig. 3 correspond to the constant pressure boundary condition ($p=90$ mmHg) and the bottom figures correspond to the resistance boundary condition ($R_i=R/|\Gamma_{Oi}|$ with $R=24000$ dyn·s/cm^5) at the outlets. In the left sub-figures, we show that the variation of the pulsating velocity at the outlets is similar to velocity profile at the inlet and the velocity at the outlets are the same for the two outlet boundary conditions. In the top-right figure, we find that for the constant pressure boundary condition the pressure at the inlet changes around 90 mmHg and its variation is similar to that of the velocity, whereas from the bottom-right figure we see that for the resistance boundary condition the pressure at the outlets are proportional to the velocity at the outlets. Compared with corresponding results of the full three-dimensional model shown in Fig. 4, we see that the waveforms are similar to each other even though the difference is visible. In the next section, we will use the corresponding matrix to construct the central-line coarse preconditioner.

4. Multiscale two-level additive Schwarz preconditioner for unsteady Stokes flows in patient-specific arteries

In this section we introduce an overlapping multiscale additive Schwarz preconditioner for the discretized system (7). The multiscale additive preconditioner takes the form $M^{-1}=M_s^{-1}+M_c^{-1}$, where M_s^{-1} is the sum of all the subdomain preconditioners and M_c^{-1} is a one-dimensional preconditioner defined on the centerline of the artery. In the following, we first briefly recall the classical additive Schwarz method and then focus on the central-line coarse preconditioner.

4.1. One-level additive Schwarz preconditioner

Denote the finite element triangulation of Ω by $\mathcal{T}_h$ and the collection of all mesh points by S_h. We partition the arterial domain Ω into N non-overlapping subdomains $\{\Omega_i\}_{i=1}^N$ such that each subdomain Ω_i consists of some elements in $\mathcal{T}_h$ denoted by $\mathcal{T}_{h,i}$. In practice, there are many ways to obtain the partition, a popular software package for partitioning an unstructured mesh is ParMETIS [51]. Extending each subdomain Ω_i with δ layers of elements from neighboring subdomains, we can obtain the overlapping subdomains $\left\{\Omega_i^\delta\right\}_{i=1}^N$ (see Fig. 5). Let $\mathcal{T}_{h,i}^\delta$ be the mesh on Ω_i^δ. For $i=1,\dots,N$, we define the following local spaces

$$\begin{aligned}
\boldsymbol{V}_h^i&=\left\{\boldsymbol{v}\in\boldsymbol{H}^1(\Omega_i^\delta):\boldsymbol{v}|_K\in P_1(K),\ \forall K\in\mathcal{T}_{h,i}^\delta;\ \boldsymbol{v}|_{\partial\Omega_i^\delta\setminus(\partial\Omega\setminus\Gamma_W)}=0;\ \boldsymbol{v}(\boldsymbol{x})=\boldsymbol{u}_I(\boldsymbol{x}),\ \forall\boldsymbol{x}\in S_h\cap\left(\partial\Omega_i^\delta\cap\Gamma_I\right)\right\},\\
P_h^i&=\begin{cases}\left\{q\in L^2(\Omega_i^\delta):q|_K\in P_1(K),\ \forall K\in\mathcal{T}_{h,i}^\delta;\ q|_{\partial\Omega_i^\delta\setminus\partial\Omega}=0;\ q|_{\partial\Omega_i^\delta\cap\Gamma_{Oj}}=p_j,\ j=1,\dots,m\right\}, & \xi=0,\\ \left\{q\in L^2(\Omega_i^\delta):q|_K\in P_1(K),\ \forall K\in\mathcal{T}_{h,i}^\delta;\ q|_{\partial\Omega_i^\delta\setminus\partial\Omega}=0\right\}, & \xi=1.\end{cases}
\end{aligned}$$

We define $R_i:\boldsymbol{V}_h\times P_h\to\boldsymbol{V}_h^i\times P_h^i$ as a restriction operator which returns all degrees of freedom associated with the subspace $V_h^i\times P_h^i$ and the transpose R_i^T of R_i as the extension operator. Denote the matrix form of the bilinear form B_ξ (7)

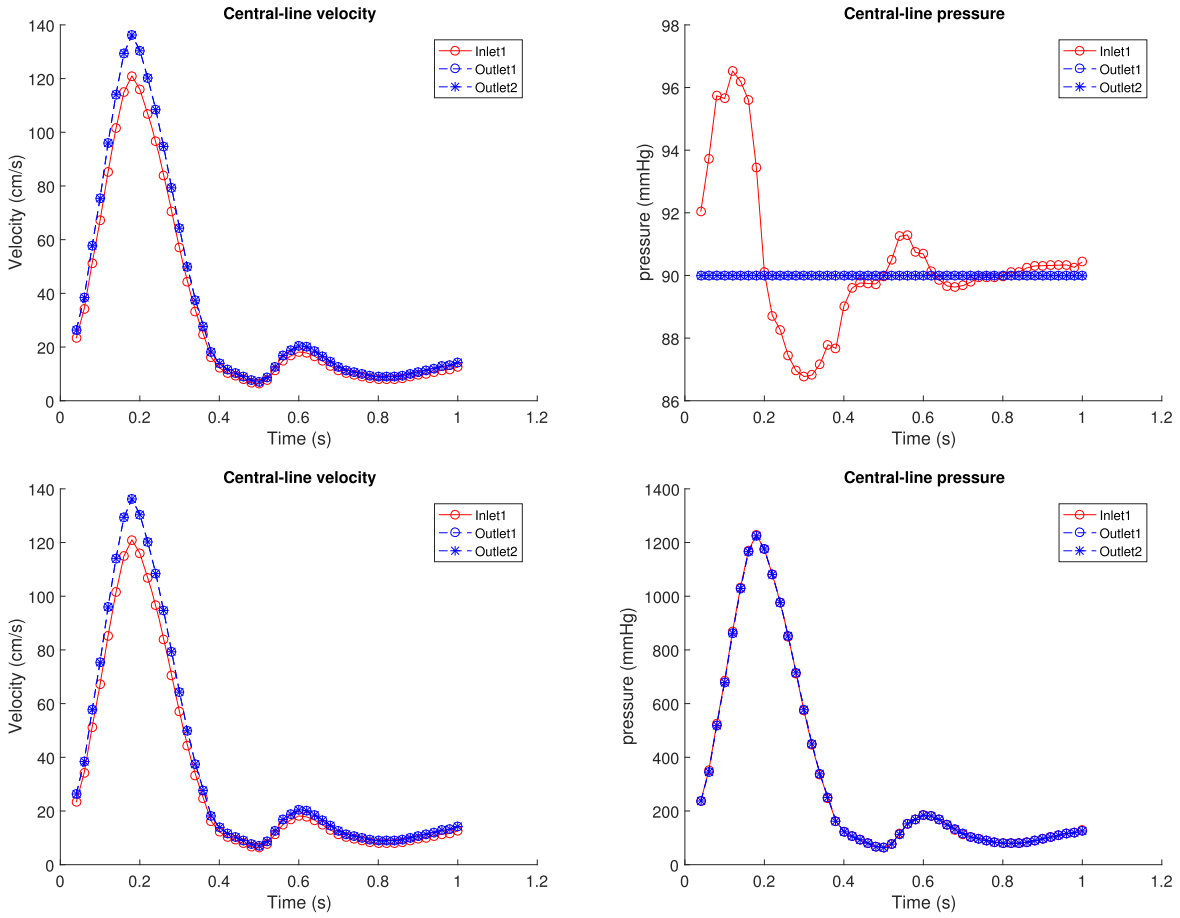

Fig. 3. Velocity and pressure curves of the parameterized one-dimensional model on the centerline of a two-branch normal artery with the constant pressure (top) or resistance (bottom) boundary condition.

as A. The subdomain matrix A_i can be obtained as $A_i = R_i A R_i^T$ or by discretizing the problem (1) on the subdomain with the corresponding conditions on the outer boundary and homogeneous Dirichlet conditions on the inner boundary. Now, the one-level additive Schwarz preconditioner in the matrix form can be described as

$$M_{1s}^{-1} = \sum_{i=1}^{N} R_i^T A_i^{-1} R_i. \tag{29}$$

Here A_i^{-1} is the subspace inverse. In practical applications, in order to reduce the communication cost and the number of iterations, one usually replace R_i^T in (29) by the corresponding extension matrix defined only in the non-overlapping subdomain, which leads to a well-known restricted additive Schwarz preconditioner [52]. Next we will introduce a central-line coarse preconditioner to further improve the effectiveness and the scalability of the one-level preconditioner.

4.2. Central-line coarse preconditioner

Let A_{cl} be the matrix form of bilinear form B_ξ^{cl} defined in (23), R_{cl} and E_{cl} the multiscale restriction and extension operators between the central-line coarse space $V_H^{cl} \times P_H^{cl}$ and the three-dimensional fine finite element space $V_h \times P_h$, respectively. Then the central-line coarse preconditioner can be written as

$$M_{cl}^{-1} = E_{cl} A_{cl}^{-1} R_{cl}. \tag{30}$$

Consequently combining the one-level preconditioner (29) with the central-line coarse preconditioner (30), we obtain the multiscale two-level additive Schwarz preconditioner

$$M_{2s,cl}^{-1} = M_{1s}^{-1} + M_{cl}^{-1} = \sum_{i=1}^{N} R_i^T A_i^{-1} R_i + E_{cl} A_{cl}^{-1} R_{cl}. \tag{31}$$

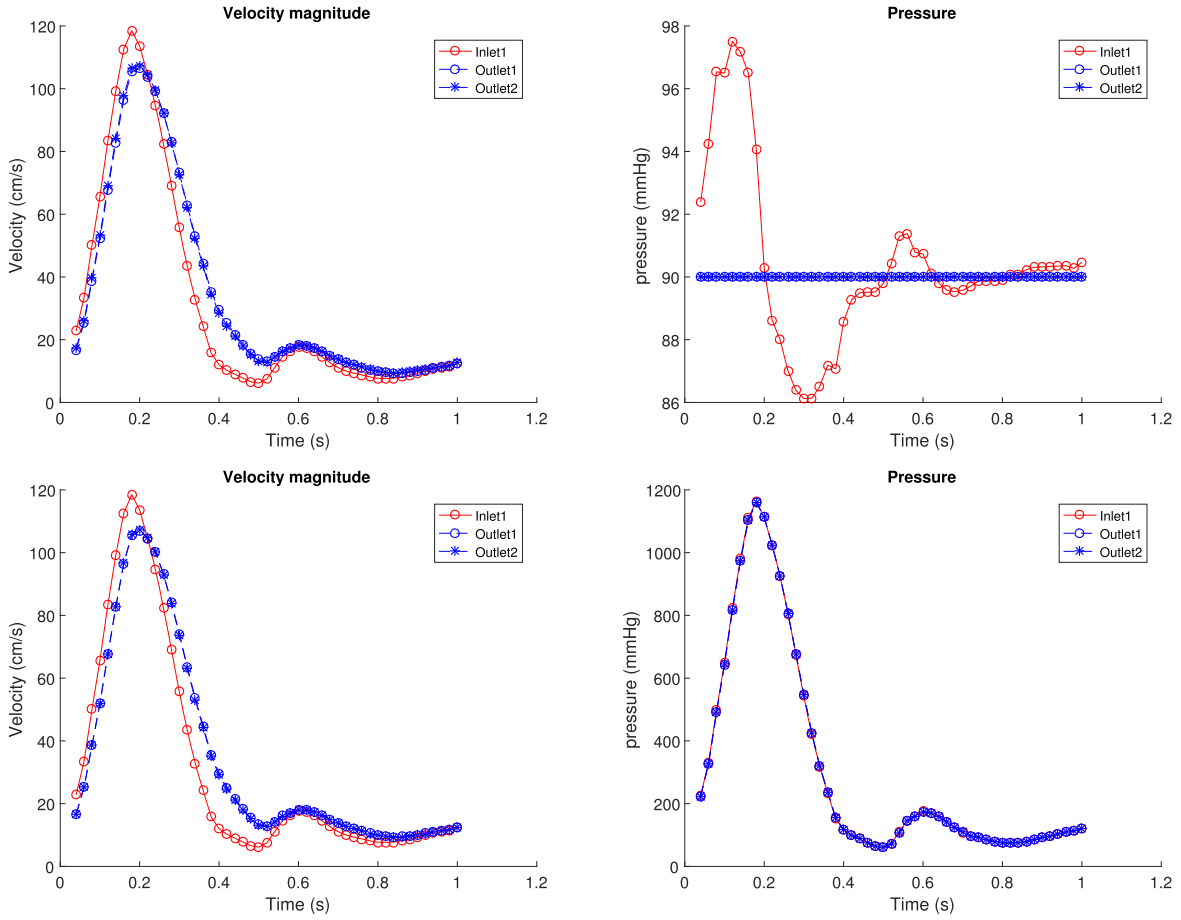

Fig. 4. Velocity magnitude and pressure of the full three-dimensional model at centers of inlet and outlets of a two-branch normal artery with the constant pressure (top) or resistance (bottom) boundary condition.

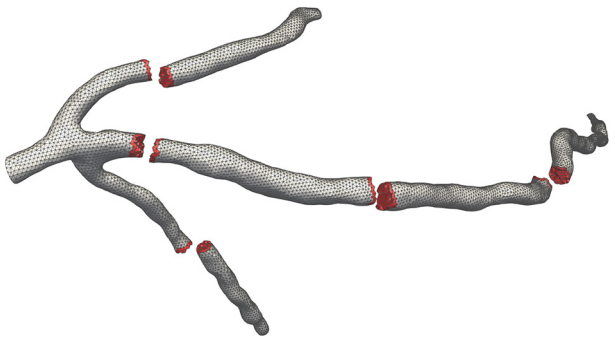

Fig. 5. Example of non-overlapping and overlapping partition of an arterial domain. The red elements represent the overlap elements with $\delta = 1$. (For interpretation of the colors in the figure(s), the reader is referred to the web version of this article.)

In the rest of this subsection, we focus on the construction of the multiscale restriction and extension operators. Let $\{\boldsymbol{x}_i\}_{i=1}^{n}$ and $\{\boldsymbol{x}(s_i)\}_{i=1}^{n_{cl}}$ be the collection of mesh points of $\mathcal{T}_h$ and $\mathcal{T}_H^{cl}$, respectively, and define the extension from (u_H^{cl}, p_H^{cl}) in $V_H^{cl} \times P_H^{cl}$ to $(\boldsymbol{u}_h, p_h)$ in $V_h \times P_h$ as

$$\boldsymbol{u}_h(\boldsymbol{x}_j) = u_H^{cl}(s)\zeta\left(\frac{|\boldsymbol{x}_j - \boldsymbol{x}(s)|}{r_0(s)}\right)\boldsymbol{\tau}(s), \quad p_h(\boldsymbol{x}_j) = p_H^{cl}(s), \tag{32}$$

for any $\boldsymbol{x}_j$ $(j = 1, \ldots, n)$ with s satisfying $\boldsymbol{x}_j \in C_s(s)$. The extension operator defined in (32) from the central-line coarse space to the three-dimensional fine mesh space is not easily computable. We next consider the matrix form of the extension

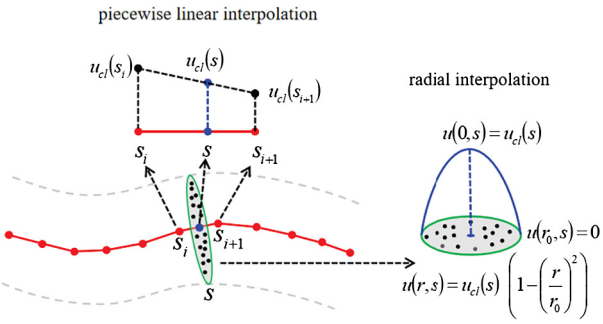

Fig. 6. Diagram of the extension processes from central-line space to three-dimensional space by radial and piecewise linear interpolations. First obtain the value of the central point (blue point) of the cross section (green section) by linear interpolation and then use it to obtain the value of mesh points (black points) included in the cross section by radial interpolation.

operator obtained by some approximations using a piecewise linear interpolation along with the centerline and a radial basis interpolation across the centerline. In Fig. 6, we show graphically the extension process in two steps: (1) first for each line segment $[s_i, s_{i+1}]$ we compute the value of the function at $s \in [s_i, s_{i+1}]$ by the piecewise linear interpolation; (2) then we compute the values of the function on the cross section $C_s(s)$ by the parabolic radial basis interpolation.

Let $\{\phi_i\}_{i=1}^{n_{cl}}$ be the nodal basis functions of P_H. For any $\boldsymbol{x}_j$, we denote by $r_j = |\boldsymbol{x}_j - \boldsymbol{x}(s)|$, where s satisfies $\boldsymbol{x}_j \in C_s(s)$. For the single vessel, let $s_{-1} = s_0, s_{n_{cl}+1} = s_{n_{cl}}$, then we call

$$D_i = \{\boldsymbol{x} \in \Omega : \boldsymbol{x} \in C_s(s) \quad \forall s \in [s_{i-1}, s_{i+1}]\},$$

as the influence region of s_i. For the artery with bifurcation, we can similarly define the influence region of s_i as D_i. Now we define the weighting $n_{cl} \times n$ matrices W^u for the velocity and W^p for the pressure as

$$W^l = \begin{pmatrix} w^l_{1,1} & \cdots & w^l_{1,n} \\ \vdots & \ddots & \vdots \\ w^l_{n_{cl},1} & \cdots & w^l_{n_{cl},n} \end{pmatrix} (l = u, p), \tag{33}$$

where the weighting coefficients $\left\{w^u_{i,j}\right\}_{i=1,j=1}^{n_{cl},n}$ and $\left\{w^p_{i,j}\right\}_{i=1,j=1}^{n_{cl},n}$ are defined as

$$w^u_{i,j} = \begin{cases} \zeta\left(\frac{r_j}{r_0}\right)\phi_i(s), & \boldsymbol{x}_j \in D_i, \boldsymbol{x}_j \in C_s(s) \\ 0, & \boldsymbol{x}_j \notin D_i \end{cases}, \quad w^p_{i,j} = \begin{cases} \psi_i(s), & \boldsymbol{x}_j \in D_i, \boldsymbol{x}_j \in C_s(s) \\ 0, & \boldsymbol{x}_j \notin D_i \end{cases},$$

and $\psi_i(s) = \phi_i(s)$ or $\psi_i(s) = 1$. We introduce $n_{cl} \times n_{cl}$ tangent matrices as

$$T_k := \operatorname{diag}\left(\tau^k(s_1), \cdots, \tau^k(s_{n_{cl}})\right) (k = 1, 2, 3), \tag{34}$$

where $\tau^k(s_i)$ is the kth component of the unit tangent vector of the centerline at the mesh point s_i defined in Section 3. Finally, using (33) and (34), we obtain the $4n \times 2n_{cl}$ extension matrix $E_{cl} : V_H^{cl} \times P_H^{cl} \to V_h \times P_h$

$$E_{cl} = \begin{pmatrix} W^u_1 & W^u_2 & W^u_3 & 0 \\ 0 & 0 & 0 & W^p \end{pmatrix}^T, \; W^u_k = T_k W^u \; (k = 1, 2, 3), \tag{35}$$

and the $2n_{cl} \times 4n$ restriction matrix $R_{cl} : V_h \times P_h \to V_H^{cl} \times P_H^{cl}$

$$R_{cl} = \begin{pmatrix} W^u_1 & W^u_2 & W^u_3 & 0 \\ 0 & 0 & 0 & W^p \end{pmatrix}, \tag{36}$$

where $\psi_i(s) = \phi_i(s)$ and $\psi_i(s) = 1$ in the definition of W^p are used for the extension and restriction matrices, respectively.

5. Numerical experiments

In this section, we present some numerical experiments to illustrate the efficiency of the central-line coarse preconditioner for unsteady Stokes flows in 3D arteries including some benchmark cases and patient-specific cases. In the simulation, we set the viscosity $\nu = 0.035$ g/(cm·s) and the source function $\boldsymbol{f} = 0$. For the inlet, we impose a pulsatile periodic flow velocity as the boundary condition with the parabolic velocity profile defined in Section 3. For the outlets, we impose the constant pressure $p_i = 90$ mmHg for the constant pressure boundary condition or the resistance $R_i = R/|\Gamma_{Oi}|$ with

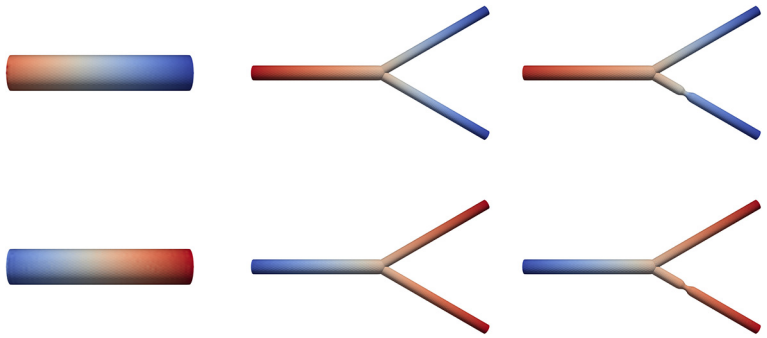

Fig. 7. Pressure distributions on the tube (left), the two-branch normal artery (middle) and the two-branch stenotic artery (right) when at $t = 0.18$ s (top) and $t = 0.5$ s (bottom).

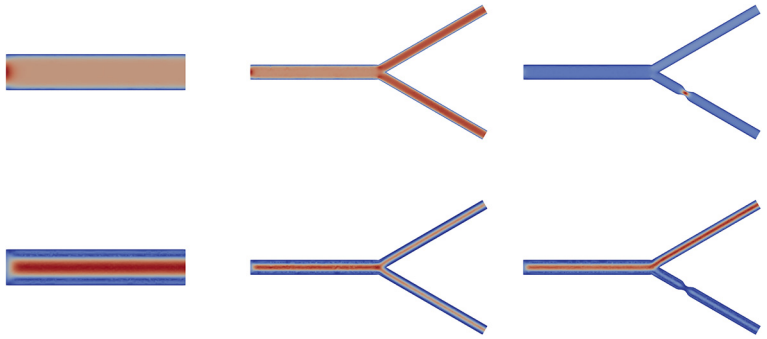

Fig. 8. Velocity distributions on the tube (left), the two-branch normal artery (middle) and the two-branch stenotic artery (right) when at $t = 0.18$ s (top) and $t = 0.5$ s (bottom).

$R = 24000$ dyn·s/cm^5 for the resistance boundary condition. The backward Euler method with a fixed time step size $\Delta t = 0.02$ s is used for the temporal discretization and the stabilized $P_1 - P_1$ finite element method with stabilization parameter $\gamma = 0.05$ is used for the spatial discretization. The fully discretized Stokes problem (7) is then solved at each time step by the right-preconditioned GMRES, which is terminated when the relative residual norm is less than or equal to 10^{-6}. In all experiments, we denote by np the number of subdomains, N as the number of mesh points. For the comparison, we show the numerical results of three preconditioners including the one-level additive Schwarz preconditioner M_1, the two-level additive Schwarz preconditioner $M_{2,c}$ whose coarse space consists of functions that are constants on each non-overlapping subdomain, and the newly proposed two-level additive Schwarz preconditioner with the central-line coarse preconditioner $M_{2,cl}$. In $M_{2,c}$, the piecewise constant coarse preconditioner can be written as $M_c^{-1} = R_c^T A_c^{-1} R_c$, where $A_c = R_c A R_c^T$ and $R_c = \text{diag}(R_{co}, R_{co}, R_{co}, R_{co})$ is a block diagonal matrix and R_{co} is a $np \times N$ matrix whose elements are either 0 or 1. More precisely, let $c_{i,j}$ be an element of R_{co}, then it takes the value 1 if the jth mesh point belongs to the ith non-overlapping subdomain; otherwise its value is 0. A two-dimensional version of the method was studied in [45].

5.1. Benchmark cases

In this subsection, we carry out experiments for three benchmark arteries including a straight tube, a two-branch normal artery and a two-branch stenotic artery to verify the proposed algorithms. For the tube, we set the radius to 0.5 cm and the length 5 cm. For the other two arteries, we set the inlet radius to 0.45 cm, the outlet radius 0.3 cm, the length of each branch 7.5 cm, and the stenotic radius 0.15 cm for the stenotic case. In the experiments, the unstructured mesh with 12542, 14344 and 11146 mesh points are considered for the tube, the two-branch normal artery and the two-branch stenotic artery, respectively. First, we show the pressure and velocity distributions for $t = 0.18$ s (peak systole) and $t = 0.50$ s (early diastole) in Fig. 7 and Fig. 8. The pressure decreases at the systole and increases at the diastole from the inlet to the outlet along the centerline and is almost a constant on each cross section. The velocity distributions are nearly symmetrical with respect to the centerline. For the two-branch case with stenosis, the velocity reaches the maximum at the stenosis at the systole, whereas at the diastole the velocity is very small. The phenomenons can also be observed for general blood flows in [53], therefore we think the new algorithms are correctly implemented.

We next study the performance of the central-line coarse preconditioner for these arteries. Since the matrices are the same for different time steps, we report the results only for the first time step, where the overlapping size $\delta = 1$, the central-line mesh with $N_{cl} = 100$ for the tube case and $N_{cl} = 238$ for the two-branch cases are the default. In Table 1, we

Table 1
The number of GMRES iterations with three different Schwarz preconditioners for the benchmark arteries, where 'AS' and 'RAS' mean additive and restricted additive Schwarz preconditioners, respectively.

Artery	np	AS						RAS					
		$\xi=0$			$\xi=1$			$\xi=0$			$\xi=1$		
		M_1	$M_{2,c}$	$M_{2,cl}$	M_1	$M_{2,c}$	$M_{2,cl}$	M_1	$M_{2,c}$	$M_{2,cl}$	M_1	$M_{2,c}$	$M_{2,cl}$
Tube	40	40	23	16	65	35	24	20	17	9	31	27	14
	80	46	26	18	73	39	27	25	21	10	38	33	16
Normal artery	40	70	27	12	105	51	24	44	24	9	57	40	16
	80	78	27	13	131	46	25	55	21	10	70	36	17
Stenotic artery	40	47	18	10	75	36	18	46	18	10	60	34	16
	80	79	25	12	112	46	21	53	23	9	73	37	16

Table 2
The effect of different sizes of the central-line mesh on the number of iterations for the benchmark arteries.

Tube			Normal artery			Stenotic artery		
N_{cl}	$\xi=0$	$\xi=1$	N_{cl}	$\xi=0$	$\xi=1$	N_{cl}	$\xi=0$	$\xi=1$
100	10	16	238	10	17	238	9	16
51	9	16	121	10	17	121	9	16
34	10	16	82	10	17	82	10	16
26	9	16	64	10	17	64	10	16
10	10	15	28	12	19	28	11	20
6	13	17	16	20	30	16	19	31
3	20	25	10	30	45	10	32	47

Table 3
The number of iterations of restricted additive Schwarz preconditioners with different overlapping sizes for the benchmark arteries.

Artery	δ	$\xi=0$			$\xi=1$		
		M_1	$M_{2,c}$	$M_{2,cl}$	M_1	$M_{2,c}$	$M_{2,cl}$
Tube	0	45	32	14	81	64	36
	1	25	21	10	38	33	16
	2	22	18	9	32	28	14
Normal artery	0	91	33	11	122	52	26
	1	55	21	10	70	36	17
	2	46	20	9	63	33	17
Stenotic artery	0	91	29	12	118	50	22
	1	53	23	9	73	37	16
	2	40	19	9	62	34	15

summarize the number of iterations of different Schwarz preconditioners and based on the results, we see clearly that both two-level preconditioners can effectively improve the convergence and scalability of the one-level preconditioner and the central-line coarse preconditioner is the fastest for all cases. From Table 1, we observe that the systems corresponding to the resistance boundary condition are more difficult to solve than the pressure boundary condition and see clearly that the restricted version performs better for all cases. Therefore, in the next two tables, we focus on the restricted additive Schwarz preconditioners.

The coarse mesh size has a significant impact on the number of iterations. By coarsening the central-line mesh, we obtain a series of central-line meshes with N_{cl} mesh points, in Table 2, we show the number of iterations by different central-line meshes. We find that a modest coarse central-line mesh is sufficient to keep the number of iterations small. Next we show results with different overlapping size δ in Table 3. Although the number of iterations decreases with increasing δ, a small overlap often produces a better result in terms of the computing time.

5.2. Patient-specific cases

In this subsection, we focus on some more complicated patient-specific arteries including a three-branch case and a twelve-branch case, as shown in Fig. 9. For the three-branch case, we consider two meshes with 331370, 1079408 mesh points, for the twelve-branch case we consider three meshes with 243013, 985457, 1497225 mesh points. In the following experiments, the overlapping size is chosen as $\delta = 1$. We restart GMRES at 30 and the stopping condition is the same as in the previous section.

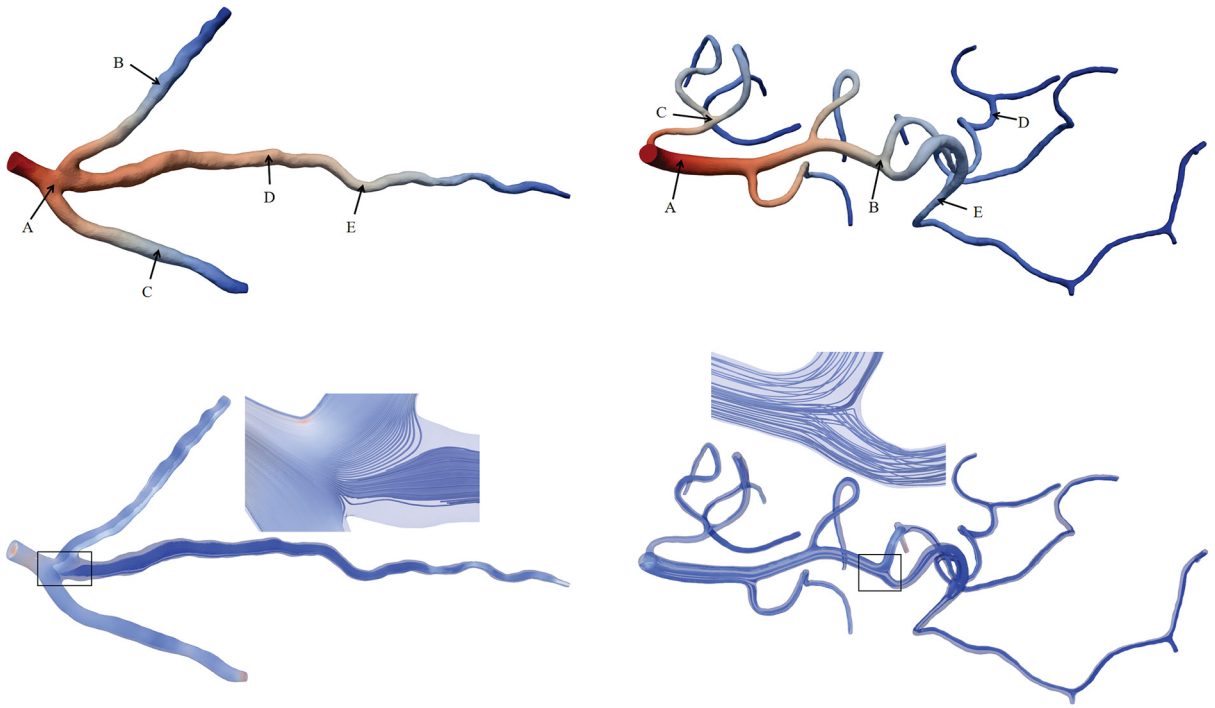

Fig. 9. Pressure distributions (top) and fluid streamlines (bottom) on the three-branch artery (left) and the twelve-branch artery (right) when $t = 0.02$ s.

Fig. 9 shows the computed pressure field and the streamlines of the velocity field on the finer meshes when $t = 0.02$ s. Fig. 10 shows the time history of pressure and velocity at five points (see marks on Fig. 9) for a heart beat with the constant pressure boundary condition. It is easy to see that the waveforms are similar at different locations, but the velocity lags behind the pressure to reach the peak and trough, and especially the pressure peak and trough appear near the maximum and minimum acceleration, respectively, which seems to be reasonable from the momentum equation when the outlet pressure is fixed. Table 4 shows the number of iterations for the additive Schwarz and the restricted additive Schwarz methods for complex arteries, where the central-line mesh with $N_{cl} = 88$ for the three-branch case and $N_{cl} = 677$ for the twelve-branch case are used for $M_{2,cl}$. The problems are harder than the benchmark problems, and some of the methods converge slowly or sometime don't converge. We observe that the number of iterations of the one-level preconditioner is very large (more than 500) for many cases, while both two-level preconditioners can greatly improve the convergence of the one-level preconditioner. For the twelve-branch artery with the resistance boundary condition, the piecewise constant coarse preconditioner performs poorly, especially for the finer mesh. We also find that the new central-line coarse preconditioner preforms well for all cases. Further in Fig. 11, we show the iteration history and the residual history. It can be seen that both two-level preconditioners have almost geometric convergence rates for the patient-specific artery, whereas the one-level method converges quickly in the first few iterations and then slowly in the later steps. We see clearly that the central-line preconditioner is robust with respect to the complex geometry of the artery.

In Table 5, we show the effect of the coarse mesh size of the central-line preconditioner on the number of iterations. We see that too many or too few mesh points both have a negative impact on the number of iterations, which may be caused by insufficient fitting for the smooth centerline or excessively interpolating from the central-line space to the three-dimensional space.

6. Conclusion

Multilevel additive Schwarz preconditioner is a useful technique in the implicit solution of the incompressible flow problem for simulating blood flows in three-dimensional arteries. However, as the geometry of the patient-specific arterial network becomes more complex, the coarse space is harder to design. Without a good coarse space, the robustness and efficiency of the preconditioned Krylov subspace suffers greatly. Thanks to the effective approximation of the one-dimensional model for blood flows in the artery, we use it to construct a simple, effective coarse preconditioner. Using the multiscale restriction and extension matrices obtained by piecewise linear and radial basis interpolations, we can integrate the central-line coarse preconditioner and the one-level additive Schwarz preconditioner into a two-level additive Schwarz preconditioner. Compared with other three-dimensional coarse preconditioners, the derivation of the preconditioner and the software implementation are more complicated, but the computational cost is much less. Note that the one-dimensional model with the assumption of axisymmetric profile and the coarse preconditioner are studied in the context of Stokes

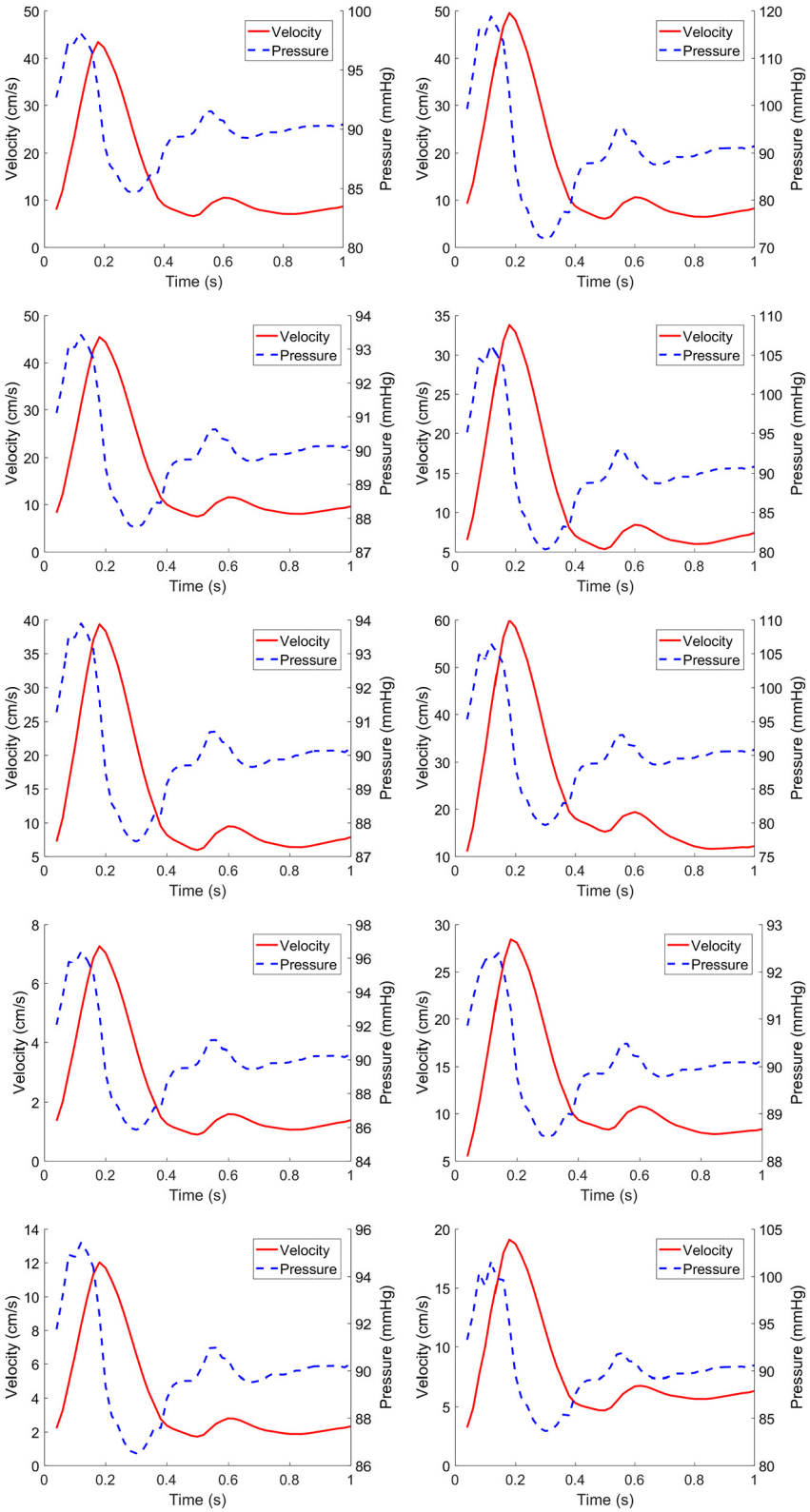

Fig. 10. The time history of pressure and velocity at five points (A, B, C, D, E) for a heart beat. Left: the three-branch artery; right: the twelve-branch artery.

Table 4
The number of GMRES iterations with three different additive Schwarz preconditioners for the patient-specific arteries, where $N_1 = 331370, N_2 = 1079408, N_3 = 243013, N_4 = 985457, N_5 = 1497225$ and '-' means the number of GMRES iterations more than 500.

Artery	N	np	AS						RAS					
			$\xi = 0$			$\xi = 1$			$\xi = 0$			$\xi = 1$		
			M_1	$M_{2,c}$	$M_{2,cl}$	M_1	$M_{2,c}$	$M_{2,cl}$	M_1	$M_{2,c}$	$M_{2,cl}$	M_1	$M_{2,c}$	$M_{2,cl}$
Three-branch artery	N_1	100	-	29	14	-	47	29	275	25	15	-	36	28
		200	-	43	19	-	59	43	388	28	17	-	47	30
		300	-	28	22	-	41	51	448	20	18	-	27	35
	N_2	300	-	28	19	-	43	48	306	19	16	-	30	36
		500	-	36	22	-	59	55	341	24	19	-	43	39
		1000	-	32	27	-	44	75	380	23	22	-	33	42
Twelve-branch artery	N_3	100	188	34	20	-	85	45	156	35	15	-	75	51
		200	-	53	23	-	135	52	237	41	16	-	82	55
		300	-	58	20	-	287	53	247	51	16	-	138	56
	N_4	300	-	57	22	-	-	54	251	40	16	-	-	52
		500	-	59	21	-	-	61	351	38	16	-	-	54
		1000	-	59	29	-	-	74	358	38	17	-	-	58
	N_5	500	-	74	20	-	-	67	338	56	15	-	-	57
		1000	-	53	25	-	-	74	430	40	17	-	-	68
		1500	-	58	26	-	-	78	451	50	18	-	-	74

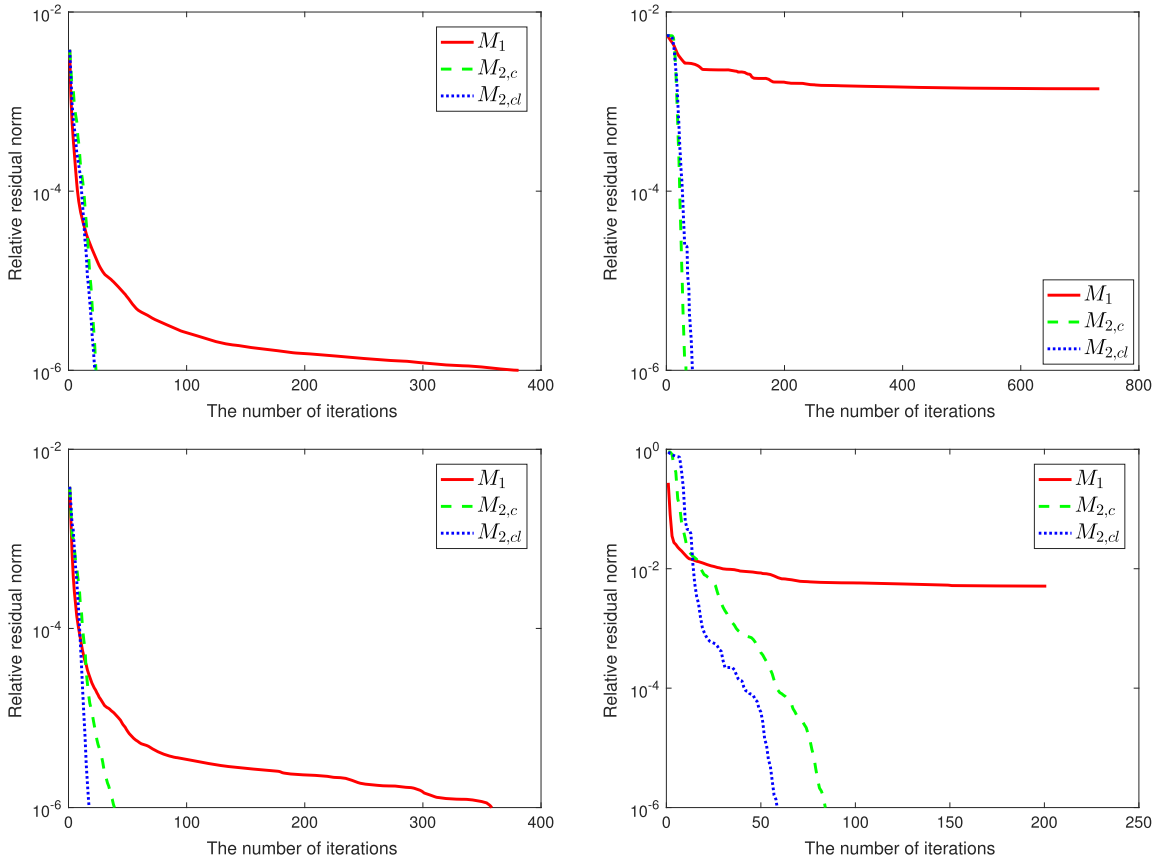

Fig. 11. The number of iterations of preconditioners for the patient-specific arteries (top: the three-branch artery; bottom: the twelve-branch artery) with the constant pressure boundary condition (left) or the resistance boundary condition (right).

equations and such a technique is useful only for artery-like domains, not for general purpose. For the general Navier-Stokes equations in hemodynamics, as the effect of the nonlinear term, the one-dimensional model may be less effective to approximate the transverse component. Consequently the performance of the central-line coarse preconditioner might be affected and need to be further investigated.

Table 5
The effect of different sizes of the central-line mesh on the number of iterations for the patient-specific arteries.

Three-branch artery			Twelve-branch artery		
N_{cl}	$\xi = 0$	$\xi = 1$	N_{cl}	$\xi = 0$	$\xi = 1$
247	14	45	1948	17	66
128	16	38	998	16	59
88	22	42	677	17	58
69	28	54	522	18	54

CRediT authorship contribution statement

Yingzhi Liu: Conceptualization, Mathematical analysis, Software, Writing. **Xiao-Chuan Cai:** Conceptualization, Methodology, Supervision.

Declaration of competing interest

We declare that we have no financial and personal relationships with other people or organizations that can inappropriately influence our work, there is no professional or other personal interest of any nature or kind in any product, service and/or company that could be construed as influencing the position presented in, or the review of, the manuscript entitled.

Data availability

No data was used for the research described in the article.

Appendix A. Supplementary material

Supplementary material related to this article can be found online at https://doi.org/10.1016/j.jcp.2023.112290.

References

[1] A. Quarteroni, M. Tuveri, A. Veneziani, Computational vascular fluid dynamics: problems, models and methods, Comput. Vis. Sci. 2 (2000) 163–197.
[2] A. Quarteroni, L. Formaggia, Mathematical modelling and numerical simulation of the cardiovascular system, Handb. Numer. Anal. 12 (2004) 3–127.
[3] A. Quarteroni, A. Manzoni, C. Vergara, The cardiovascular system: mathematical modelling, numerical algorithms and clinical applications, Acta Numer. 26 (2017) 365–590.
[4] Z. Lin, R. Chen, B. Gao, S. Qin, B. Wu, J. Liu, X.-C. Cai, A highly parallel simulation of patient-specific hepatic flows, Int. J. Numer. Methods Biomed. Eng. 37 (2021) e3451.
[5] S. Qin, B. Wu, J. Liu, W.-S. Shiu, Z. Yan, R. Chen, X.-C. Cai, Efficient parallel simulation of hemodynamics in patient-specific abdominal aorta with aneurysm, Comput. Biol. Med. 136 (2021) 104652.
[6] S. Qin, B. Wu, J. Liu, W.-S. Shiu, Z. Yan, R. Chen, X.-C. Cai, Numerical simulation of blood flows in patient-specific abdominal aorta with primary organs, Biomech. Model. Mechanobiol. 20 (2021) 909–924.
[7] L. Luo, W.-S. Shiu, R. Chen, X.-C. Cai, A nonlinear elimination preconditioned inexact Newton method for blood flow problems in human artery with stenosis, J. Comput. Phys. 399 (2019) 108926.
[8] R. Chen, B. Wu, Z. Cheng, W.-S. Shiu, J. Liu, L. Liu, Y. Wang, X. Wang, X.-C. Cai, A parallel non-nested two-level domain decomposition method for simulating blood flows in cerebral artery of stroke patient, Int. J. Numer. Methods Biomed. Eng. 36 (2020) e3392.
[9] V.L. Streeter, W.F. Keitzer, D.F. Bohr, Pulsatile pressure and flow through distensible vessels, Circ. Res. 13 (1963) 3–20.
[10] A.H. Shapiro, Steady flow in collapsible tubes, J. Biomech. Eng. 99 (1977) 126–147.
[11] L. Formaggia, F. Nobile, A. Quarteroni, A. Veneziani, Multiscale modelling of the circulatory system: a preliminary analysis, Comput. Vis. Sci. 2 (1999) 75–83.
[12] S. Sherwin, V. Franke, J. Peiro, K. Parker, One-dimensional modelling of a vascular network in space-time variables, J. Eng. Math. 47 (2003) 217–250.
[13] L. Formaggia, D. Lamponi, A. Quarteroni, One-dimensional models for blood flow in arteries, J. Eng. Math. 47 (2003) 251–276.
[14] N. Smith, A. Pullan, P. Hunter, An anatomically based model of transient coronary blood flow in the heart, SIAM J. Appl. Math. 62 (2002) 990–1018.
[15] J. Lee, N. Smith, Development and application of a one-dimensional blood flow model for microvascular networks, Proc. Inst. Mech. Eng., H J. Eng. Med. 222 (2008) 487–511.
[16] L. Formaggia, F. Nobile, A. Quarteroni, A one dimensional model for blood flow: application to vascular prosthesis, in: Mathematical Modeling and Numerical Simulation in Continuum Mechanics, Springer, 2002, pp. 137–153.
[17] S. Čanić, Blood flow through compliant vessels after endovascular repair: wall deformations induced by the discontinuous wall properties, Comput. Vis. Sci. 4 (2002) 147–155.
[18] S. Sherwin, L. Formaggia, J. Peiro, V. Franke, Computational modelling of 1D blood flow with variable mechanical properties and its application to the simulation of wave propagation in the human arterial system, Int. J. Numer. Methods Fluids 43 (2003) 673–700.
[19] L. Formaggia, J.-F. Gerbeau, F. Nobile, A. Quarteroni, On the coupling of 3D and 1D Navier–Stokes equations for flow problems in compliant vessels, Comput. Methods Appl. Mech. Eng. 191 (2001) 561–582.
[20] S. Perotto, A. Ern, A. Veneziani, Hierarchical local model reduction for elliptic problems: a domain decomposition approach, Multiscale Model. Simul. 8 (2010) 1102–1127.
[21] L. Mansilla Alvarez, P. Blanco, C. Bulant, E. Dari, A. Veneziani, R. Feijóo, Transversally enriched pipe element method (TEPEM): an effective numerical approach for blood flow modeling, Int. J. Numer. Methods Biomed. Eng. 33 (2017) e2808.
[22] S. Guzzetti, S. Perotto, A. Veneziani, Hierarchical model reduction for incompressible fluids in pipes, Int. J. Numer. Methods Eng. 114 (2018) 469–500.

[23] Y.A. Brandes Costa Barbosa, S. Perotto, Hierarchically reduced models for the Stokes problem in patient-specific artery segments, Int. J. Comput. Fluid Dyn. 34 (2020) 160–171.
[24] N. Xiao, J. Alastruey, C. Alberto Figueroa, A systematic comparison between 1-D and 3-D hemodynamics in compliant arterial models, Int. J. Numer. Methods Biomed. Eng. 30 (2014) 204–231.
[25] L. Grinberg, E. Cheever, T. Anor, J.R. Madsen, G. Karniadakis, Modeling blood flow circulation in intracranial arterial networks: a comparative 3D/1D simulation study, Ann. Biomed. Eng. 39 (2011) 297–309.
[26] P. Reymond, F. Perren, F. Lazeyras, N. Stergiopulos, Patient-specific mean pressure drop in the systemic arterial tree, a comparison between 1-D and 3-D models, J. Biomech. 45 (2012) 2499–2505.
[27] D.M. Sforza, C.M. Putman, J.R. Cebral, Hemodynamics of cerebral aneurysms, Annu. Rev. Fluid Mech. 41 (2009) 91–107.
[28] J.H. Bramble, J.E. Pasciak, A.T. Vassilev, Analysis of the inexact Uzawa algorithm for saddle point problems, SIAM J. Numer. Anal. 34 (1997) 1072–1092.
[29] H.C. Elman, G.H. Golub, Inexact and preconditioned Uzawa algorithms for saddle point problems, SIAM J. Numer. Anal. 31 (1994) 1645–1661.
[30] L. Formaggia, J.-F. Gerbeau, F. Nobile, A. Quarteroni, Numerical treatment of defective boundary conditions for the Navier-Stokes equations, SIAM J. Numer. Anal. 40 (2002) 376–401.
[31] A. Quarteroni, F. Saleri, A. Veneziani, Analysis of the Yosida method for the incompressible Navier-Stokes equations, J. Math. Pures Appl. (9) 78 (1999) 473–503.
[32] A. Quarteroni, F. Saleri, A. Veneziani, Factorization methods for the numerical approximation of Navier-Stokes equations, Comput. Methods Appl. Mech. Eng. 188 (2000) 505–526.
[33] J.L. Guermond, P. Minev, J. Shen, An overview of projection methods for incompressible flows, Comput. Methods Appl. Mech. Eng. 195 (2006) 6011–6045.
[34] A. Klawonn, An optimal preconditioner for a class of saddle point problems with a penalty term, SIAM J. Sci. Comput. 19 (1998) 540–552.
[35] A. Klawonn, Block-triangular preconditioners for saddle point problems with a penalty term, SIAM J. Sci. Comput. 19 (1998) 172–184.
[36] A. Klawonn, L.F. Pavarino, Overlapping Schwarz methods for mixed linear elasticity and Stokes problems, Comput. Methods Appl. Mech. Eng. 165 (1998) 233–245.
[37] A. Klawonn, L.F. Pavarino, A comparison of overlapping Schwarz methods and block preconditioners for saddle point problems, Numer. Linear Algebra Appl. 7 (2000) 1–25.
[38] L.F. Pavarino, Indefinite overlapping Schwarz methods for time-dependent Stokes problems, Comput. Methods Appl. Mech. Eng. 187 (2000) 35–51.
[39] L.F. Pavarino, O. Widlund, Balancing Neumann-Neumann methods for incompressible Stokes equations, Commun. Pure Appl. Math. 55 (2002) 302–335.
[40] J. Li, O. Widlund, BDDC algorithms for incompressible Stokes equations, SIAM J. Numer. Anal. 44 (2006) 2432–2455.
[41] J. Li, A dual-primal FETI method for incompressible Stokes equations, Numer. Math. 102 (2005) 257–275.
[42] H.H. Kim, C.-O. Lee, E.-H. Park, A FETI-DP formulation for the Stokes problem without primal pressure components, SIAM J. Numer. Anal. 47 (2010) 4142–4162.
[43] F. Kong, X.-C. Cai, A highly scalable multilevel Schwarz method with boundary geometry preserving coarse spaces for 3D elasticity problems on domains with complex geometry, SIAM J. Sci. Comput. 38 (2016) C73–C95.
[44] F. Kong, X.-C. Cai, A scalable nonlinear fluid–structure interaction solver based on a Schwarz preconditioner with isogeometric unstructured coarse spaces in 3D, J. Comput. Phys. 340 (2017) 498–518.
[45] Y. Liu, X.-C. Cai, A central-line coarse preconditioner for Stokes flows in artery-like domains, Numer. Algorithms 87 (2021) 137–160.
[46] Y. Liu, F. Qi, X.-C. Cai, A one-dimensional coarse preconditioner for three-dimensional unsteady incompressible Navier-Stokes flows in patient-specific arteries, SIAM J. Sci. Comput. (2022).
[47] P.B. Bochev, M.D. Gunzburger, J.N. Shadid, On inf–sup stabilized finite element methods for transient problems, Comput. Methods Appl. Mech. Eng. 193 (2004) 1471–1489.
[48] T. Barth, P. Bochev, M. Gunzburger, J. Shadid, A taxonomy of consistently stabilized finite element methods for the Stokes problem, SIAM J. Sci. Comput. 25 (2004) 1585–1607.
[49] P. Grisvard, Elliptic Problems in Nonsmooth Domains, SIAM, 2011.
[50] H. Sohr, The Navier-Stokes Equations: An Elementary Functional Analytic Approach, Springer Science & Business Media, 2012.
[51] G. Karypis, V. Kumar, Multilevel k-way partitioning scheme for irregular graphs, J. Parallel Distrib. Comput. 48 (1998) 96–129.
[52] X.-C. Cai, M. Sarkis, A restricted additive Schwarz preconditioner for general sparse linear systems, SIAM J. Sci. Comput. 21 (1999) 792–797.
[53] I.E. Vignon-Clementel, C.A. Figueroa, K.E. Jansen, C.A. Taylor, Outflow boundary conditions for three-dimensional finite element modeling of blood flow and pressure in arteries, Comput. Methods Appl. Mech. Eng. 195 (2006) 3776–3796.